RESEARCH ARTICLE

MERIDA HRES: A new high-resolution reanalysis dataset for Italy

Francesca Viterbo[1] 🔵 | Simone Sperati[1] | Bruno Vitali[1] | Filippo D'Amico[1] |
Francesco Cavalleri[2] | Riccardo Bonanno[1] | Matteo Lacavalla[1]

[1]Ricerca sul Sistema Energetico (RSE)
S.p.A, Milan, Italy

[2]Environmental Science and Policy
Department, University of Milan, Milan,
Italy

Correspondence
Francesca Viterbo, Ricerca sul Sistema
Energetico (RSE) S.p.A., Milan, Italy.
Email: francesca.viterbo@rse-web.it

Funding information
Research Fund for the Italian Electrical
System; PNRR funds (from the EU Next-
generation programme)

Abstract

Power utilities are increasingly emphasizing the need for high-resolution reanalysis datasets to develop resilience plans for protecting and managing infrastructure against extreme weather events. In response, Ricerca Sul Sistema Energetico (RSE) S.p.A. created the new MEteorological Reanalysis Italian DAtaset (MERIDA) High-RESolution (HRES) reanalysis, a 4-km resolution dataset with explicit convection specifically designed for Italy. This dataset, publicly available from 1986 to the present, has been evaluated and compared with the previously developed MERIDA reanalysis dataset (7-km resolution over Italy) and ERA5, the global reanalysis driver. The validation is conducted across different scales (i.e., from climatology to single extreme events) and for multiple variables (i.e., 2-meter temperature, daily total precipitation, and 10-meter wind speed). Specific cases, such as a convective storm in July 2016 in northern Italy near Bergamo and the more synoptically driven Vaia storm in October 2018, are analyzed to illustrate the dataset's potential in capturing precipitation and wind extremes. Additionally, the Arbus wildfire event in Sardinia is examined to showcase a multivariable application for assessing fire weather hazards. Through performance maps and statistical analyses, the ability of MERIDA HRES to represent both long-term statistics and extreme events is highlighted. Despite a consistent cold temperature bias across Italy, with higher peaks over mountainous regions, the performance of precipitation and wind outperforms that of both MERIDA and ERA5 in all analyzed cases. These findings demonstrate the significant potential of this product for multiple applications in Italy.

KEYWORDS

extreme events, Italy, power system resilience, reanalyses validation, regional reanalyses, WRF

1 | INTRODUCTION

Reanalysis products combine information from Numerical Weather Prediction models (NWP) and weather observations (weather satellites, surface and upper air stations, weather radar, etc.) to reproduce past weather and climate conditions in the most accurate way possible (Kalnay, 1996). Reanalysis datasets can compensate for the lack of observations in areas with few or no stations, or where certain variables are hard to measure, using a physically based atmospheric model that calculates spatially distributed atmospheric fields and improves accuracy through the assimilation of meteorological data. Reanalyses provide spatially distributed and temporally consistent atmospheric information on a grid, spanning multiple years and several vertical levels. They also help to describe soil variables, such as soil moisture and temperature, that are difficult to observe with generally very low-density observation networks. This information is used by scientists, policymakers, and stakeholders to adapt to climate change and extreme weather events, including recent advances in using reanalysis data to train AI forecasting models (Dueben & Bauer, 2018; Weyn et al., 2019). In the energy sector, reanalyses are powerful tools for investigating the availability of renewable sources and estimating their producibility and for supporting the evaluation of power system resilience in terms of operational planning (Bloomfield et al., 2021; Craig et al., 2022; Kies et al., 2021; Troccoli et al., 2014).

In many parts of the world, power utilities, governments, and other stakeholders have solicited the use of high-resolution reanalysis datasets to investigate past climate variability and trends and to reconstruct specific test cases that had significant repercussions on the availability of resources and the quality of the energy supply. For example, the American Meteorological Society (AMS) Policy Program Study on "Actionable Scientific Assessments for the Energy Sector" in the United States stressed the need for comprehensive and continuously updated high-resolution reanalyses, with resolutions from 4 to 1 km, to fully integrate meteorological and energy information for electric stakeholders (Tipton & Seitter, 2022). Additionally, in Europe, climate services, such as Copernicus, have developed reanalysis-based platforms for the energy industry and policymakers to provide time series of electricity demand and supply from wind, solar, photovoltaic, and hydropower sources, such as the C3S energy service (Dubus et al., 2023). In addition, many studies over the European domain have stressed the need to use reanalyses at resolutions higher than those of ERA5 (Hersbach et al., 2020) to perform studies on the availability of wind and solar radiation across Europe (Camargo et al., 2019; Victoria &

Andresen, 2019). Additionally, in Italy, the Power Utilities (Transmission System Operator-TSO and Distribution System Operators-DSOs) have solicited similar questions to enhance the resilience of the electrical system and improve the estimation of renewable energy sources. For example, in 2017, ARERA, the Italian Regulatory Authority for Energy, Networks and Environment, issued a consultation document (645/2017/R/EEL) in which it is envisaged that the analysis of power system resilience is based on meteorological reanalysis datasets (ARERA, 2017).

To answer these needs, ARERA instructed Ricerca sul Sistema Energetico (RSE) S.p.A. to develop a reanalysis product that can provide a common meteorological dataset for the energy sector. From this original assignment, in 2019, the MEteorological Reanalysis Italian DAtaset (MERIDA) reanalysis and the MERIDA Optimal Interpolation (OI) dataset were created, with a 7-km spatial resolution and a 1-h temporal resolution over Italy (Bonanno et al., 2019).

Since then, MERIDA reanalysis has been used for several studies and applications on the energy system. For example, in the paper of Bonanno and Lacavalla (2020), the MERIDA surface temperature, soil temperature, and moisture at different soil depths were used to develop a prototype alerting system for distribution Medium Voltage underground cables. On the electrical transmission grid, however, many studies have used MERIDA to investigate the impact of wet snow falls on the formation of snow sleeves on overhead conductors from both an operational planning perspective and a future scenario perspective (Amicarelli et al., 2019; Faggian et al., 2021; Faggian et al., 2024; Lacavalla et al., 2019; Lacavalla et al., 2022). For wind power generation, MERIDA was used to bias correct 10-m wind speed from Euro-CORDEX regional climate models to highlight the areas in Italy in which wind producibility is expected to increase (Bonanno et al., 2023). Finally, in the study by Faggian and Trevisiol (2024), different extreme climate scenarios (i.e., drought conditions, strong winds, heavy rainfalls) were analyzed with a multihazard approach, where MERIDA provided a benchmark for the past climate for the periods 1986–2005 and 2006–2019 (Faggian & Trevisiol, 2024). In addition, the MERIDA variables of temperature and precipitation were analyzed in the papers of Stefanini et al. (2023) and Capozzi et al. (2023), respectively, for local assessment studies over Italy, and they were also used as forcings for hydrological models (Abbate et al., 2024).

All these examples demonstrated the ability of MERIDA to correctly describe atmospheric variables and to represent physical processes and their impacts on multiple spatial and temporal scales.

In the following years, many other products of regional reanalysis, specifically available over Italy and/or Europe, became available at a similar resolution as MERIDA over Italy. At the European level, for example, the ECMWF released the CERRA reanalysis, forced by ERA5, with outputs at 5.5 km over the whole Europe (Verrelle et al., 2022). In Italy, both SPHERA and VHR-REA-IT use the COSMO model to perform reanalysis products over Italy at 2.2 km (Cerenzia et al., 2022; Raffa et al., 2021). Some studies, such as the work of Cavalleri et al. (2024), compared the different reanalysis products across Italy for certain variables of interest, highlighting the potential and limitations of each product.

The constant push toward higher resolutions and the need to constantly develop new reanalysis products with updated parameterizations created the opportunity to give birth to another additional dataset. In 2022, RSE developed the Atlante EOLico ItaliANo (AEOLIAN) dataset, a wind atlas at 1.3 km that offers promising results for representing high-resolution wind speeds across the Italian territory (Sperati et al., 2024). In the process, another fully physically based reanalysis, at a higher resolution than MERIDA, with a 4-km resolution and updated parameterizations, called MERIDA High-RESolution (HRES), was created. MERIDA HRES, in fact, provided the Initial Conditions (IC) and Boundary Conditions (BC) for AEOLIAN dynamical downscaling. This reanalysis, nevertheless, was not limited to a mere IC and BC for the AEOLIAN dataset; instead, it has been fully developed, offering a plethora of variables at higher resolution than MERIDA and with some significant parameterization updates from the first creation of the MERIDA dataset.

As this dataset is available publicly at https://merida.rse-web.it/[1] and offers information at 4 km for the period from 1986 to present[2] across Italy, this study aims to present this new product to the scientific community. Evaluations are conducted on various variables and scales to demonstrate the potential of applying this new dataset in Italy for applications where interactions between physically based variables are crucial for predicting impacts on the surface, such as in complex terrain or coastal areas, and in fields requiring higher resolution, like hydrology, wildfires, and convective storms. In particular, the results for MERIDA HRES are evaluated considering multiple variables of interest, such as precipitation, temperature, and wind, at different spatial and temporal scales. MERIDA HRES is compared against MERIDA reanalysis,

which represents a previous development and the actual state-of-the-art of reanalysis produced in RSE, and with ERA5 global reanalysis, which is the driver of both MERIDA and MERIDA HRES. The performances are validated by comparing the reanalysis datasets with point and gridded observations via spatially distributed performance maps and by calculating statistical summary scores for the different variables. The validation is performed over multiple years to assess the ability of the reanalyses to represent the climatology of Italy for those variables of interest and at the scale of a single event to explore whether the MERIDA HRES is also able to represent extremes in precipitation and wind. At the event scale, this is illustrated with two cases: a summer convective storm on July 31, 2016, which caused heavy rainfall in the central Alps foothills near Bergamo, and the more synoptically driven Vaia storm, which affected the northeast Alpine regions of Veneto and Trentino from October 28 to November 2, 2018. Vaia's strong winds damaged 67,000 km^2 of forested areas (Giannetti et al., 2021) and caused widespread power outages due to fallen trees on power lines. Finally, to provide a demonstrative example of a possible multivariable application of the MERIDA HRES reanalysis, a calculation of fire weather hazard is presented for a wildfire event on Sardinia Island (i.e., the Arbus wildfire of July 2016).

After this introductory paragraph, Section 2 provides a description of MERIDA HRES (Section 2.1) and the observations used in the comparisons (Section 2.2). Section 3 describes the results obtained for the comparison for every variable analyzed, both on multiple years (Section 2.1) and at the event scale (Section 2.2). Finally, Section 4 presents the conclusions of the analyses.

2 | DATA AND METHODS

The evaluation of MERIDA HRES and the comparison with its predecessor MERIDA and the ERA5 driver are conducted for multiple variables, including 2-m temperature (t2m), daily total precipitation, and 10-m wind speed, and across various scales, from climatology to single-event analysis. Specifically, t2m and precipitation are analyzed using gridded observations from 2000 to 2020 and station data from 2016 to 2020. Wind speed at 10 m is compared with anemometer stations over several years across Italy. Additionally, specific precipitation and wildfire events are examined using multiple observation sources, as detailed in Section 2.2. To improve readability, information on the methodologies, skill scores, and other relevant details are included within the Results sections: multi-year evaluation in Section 2.1, and individual event assessments in Section 2.2.

---

[1]MERIDA HRES is publicly available at the web platform https://merida.rse-web.it/. This website is the same platform where also MERIDA is available.

[2]At the moment of writing, MERIDA HRES is available up to 2022, but it is extended yearly for additional 12 months.

In the present Section (Section 2), a detailed description of the MERIDA HRES product is given, including parameterizations choices and physics settings (Section 2.1), whereas an overview of the stations and gridded observations used for the multiyear comparison is given in Section 2.2.1 and Section 2.2.2, respectively.

2.1 | MERIDA HRES reanalyses

MERIDA HRES reanalyses involve dynamical downscaling of the ERA5 global reanalysis (Hersbach et al., 2020) via the WRF-ARW-V3.9 mesoscale model (Skamarock et al., 2008) at a spatial resolution of 4 km, producing outputs at a 1-h temporal resolution for the period from 1986 to present[2]. ERA5 provides BCs every hour to ensure good temporal consistency between the ERA5 global model and the WRF dynamical downscaling. In addition, surface temperature data at 2 m from SYNOP stations are assimilated every 3 h, with the same observational nudging technique adopted in MERIDA (Bonanno et al., 2019). A 50-km radius of influence is defined around each SYNOP station. The difference between the model and the observed data, known as the "innovation term", is multiplied by a standard nudging coefficient and added to the model's predictive equations. This process gradually adjusts the model toward the observed data.

Because the MERIDA HRES reanalysis was originally developed to provide IC and BC for the AEOLIAN dataset, a complete description of the WRF-ARW settings and the parameterization choices is given in the paper of Sperati et al. (2024) (where the MERIDA HRES physics options coincide with those used for the external domain of the simulation) and is summarized in Table 1. Overall, the methodology used to develop the MERIDA HRES dynamical downscaling has many similarities with the MERIDA reanalysis (whose specific settings are described in Bonanno et al. (2019)), even if there are some important differences in the choice of physics settings and parametrizations, described hereinafter:

- MERIDA HRES has a resolution of 4 km, whereas MERIDA has a resolution of 7 km. MERIDA HRES resolution resolves explicit convection, instead of parameterized convection, as in MERIDA. The 4-km resolution describes the so-called "gray zone" (Honnert et al., 2020; Wyngaard, 2004), where it is reasonable to abandon parametrizations and directly resolve convection.
- Compared with MERIDA, MERIDA HRES has an increased number of vertical levels, to improve the representation of wind in the planetary boundary layer.

TABLE 1 Physics schemes selected in the configuration of WRF-ARW for MERIDA HRES reanalysis.

Physics	Scheme
Microphysics	Thompson (Thompson et al., 2008)
Long-wave radiation	RRTMG (Iacono et al., 2008)
Short-wave radiation	RRTMG
Surface layer	Revised MM5 Monin-Obukhov (Jiménez et al., 2012)
Planetary boundary layer (PBL)	Yonsei University (Hong et al., 2006)
Land surface	NOAH-MP (Niu et al., 2011 ; Yang et al., 2011)
Land use	USGS 28 category (Anderson et al., 1976)
Soil classes	Food and Agricultural Organization (FAO) (Miller & White, 1998)
Cumulus scheme	Off
Surface drag	topo_wind = 1 (Jimenez & Dudhia, 2012)

While they both have the model top at 50 hPa, MERIDA has 44 vertical levels, whereas MERIDA HRES has 56 vertical levels, with an increased vertical resolution at the lower levels (located at 10, 35, 70, 100, 130, 180, 250, 325, 415, and 500 m).

- In addition, to decrease the positive wind bias at 10 m typically observed in WRF-ARW simulations, MERIDA HRES, and consequently AEOLIAN, uses the option topo_wind = 1 in the WRF namelist to set the surface drag parameterization properly (Jimenez & Dudhia, 2012).
- The MERIDA HRES domain consists of 520 × 520 grid points to cover all of Italy and the Mediterranean area. The domain is significantly wider than the MERIDA geographic domain to allow lateral fluxes from the BC to propagate from the boundaries to the center of the domain (where the Italian region is located) and to develop their own physics (Figure 1). In addition, spectral nudging (von Storch et al., 2000) is used, as in MERIDA, to filter synoptic perturbations at smaller scales and to avoid introducing spurious signals into the model simulation from the ERA5 global model.
- MERIDA HRES uses the Noah-MP Land Surface Model (LSM) (Niu et al., 2011; Yang et al., 2011) instead of the Noah LSM (Mitchell, 2005), as used in MERIDA. Noah-MP multi-physics is designed to allow a better representation of moist and heat fluxes than those predicted by the Noah LSM, especially for vegetation ecology, snow representation, and groundwater (Ju et al., 2022).
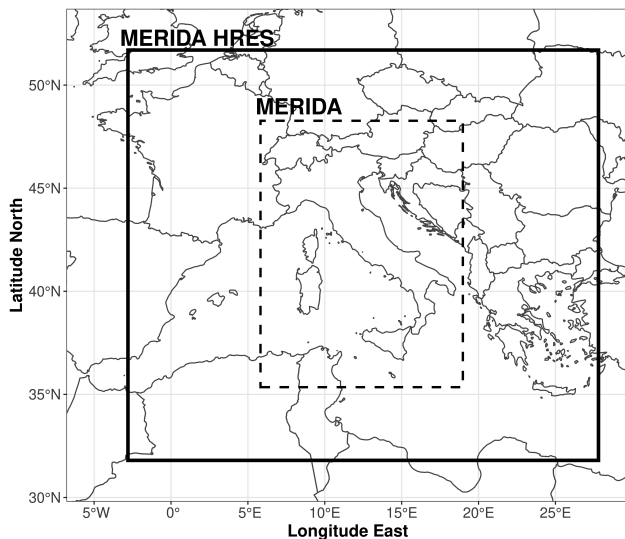
FIGURE 1 Computational domain of the MERIDA HRES (solid line) and MERIDA (dashed line) simulations.

- In MERIDA HRES, aerosols are assimilated in the WRF simulations via the Aerosol Optical Depth (AOD), Angstrom exponent and Single Scattering Albedo from the MERRA2 reanalysis every 3 h via the Ruiz-Arias method (Ruiz-Arias et al., 2013).

These modifications to the original MERIDA physical parametrization were designed to maximize the accuracy of the wind variable for AEOLIAN, intended as a wind atlas. However, these design choices could also positively affect other variables. For instance, using Noah-MP instead of Noah can improve the representation of heat and moisture fluxes, enhance land–atmosphere coupling, and strengthen evapotranspiration feedbacks to the atmosphere, potentially leading to a better representation of convective events, where localized evapotranspiration plays a key role in triggering convection. Additionally, running the WRF-ARW model with explicit convection can improve the representation of convection and the initiation of localized storms (especially frequent in Italy during the summer) where convection is crucial, and convection-permitting simulations are expected to perform better than those using parameterization.

In this study, an extensive validation of the MERIDA HRES is performed to prove how this reanalysis product can be used for multiple applications other than wind only (as already proven in AEOLIAN development (Sperati et al., 2024)). The evaluation is performed considering multiple variables, such as 2-m temperature, 10-m wind speed and precipitation, and compares the MERIDA HRES reanalyses with MERIDA and with their common driver ERA5, calculating their skills through a comparison with available observations (point and gridded). In the following paragraph (Section 2.2), a brief

description of the observation datasets and the methodology used in the comparison are given.

2.2 | Observational datasets

Validating a reanalysis product on multiple variables requires different sources of observations. A brief description of the station observations and the gridded dataset used in the comparison is given in the following paragraphs.

2.2.1 | Stations

Point-based observations are used to compare each reanalysis field with the measured variables at a specific location. The comparisons for 2-m temperature and precipitation are performed via the same observing meteorological stations from the Regional Agencies for Environmental Protection (ARPA) (Italian Civil Protection Department and CIMA Research Foundation, 2014), which are homogeneously distributed across Italy, as already shown in Bonanno & Lacavalla, 2020. Criteria of temporal and spatial consistency were applied to validate the quality of the observational data for the comparisons, in the same way as in MERIDA (Bonanno & Lacavalla, 2020).

To ensure a more consistent distribution of stations across all Italian regions, the statistical comparisons of temperature and precipitation are performed over the period 2016–2020. Before 2016, some regions of Italy lacked or had limited data for temperature and precipitation, making earlier periods less reliable for comparison or less representative of the entire spatial domain.

Wind comparisons are performed via the same 94 anemometers for 10-m winds used in the study of Sperati et al. (2024), which were distributed across the Italian territory. In this case, the statistical verification was performed using the maximum available time-series length, with a minimum requirement of at least 2 years of continuous records in the period 2010–2020 for each station. Figure 2 shows the geographical location of the wind observations considered.

2.2.2 | Gridded

In addition to using point-based observations, t2m and precipitation climatology are evaluated considering gridded datasets to investigate spatial distributions and patterns. In fact, especially for precipitation, the spatial distribution and pattern play important roles in understanding the type of event (e.g., synoptic or convective)
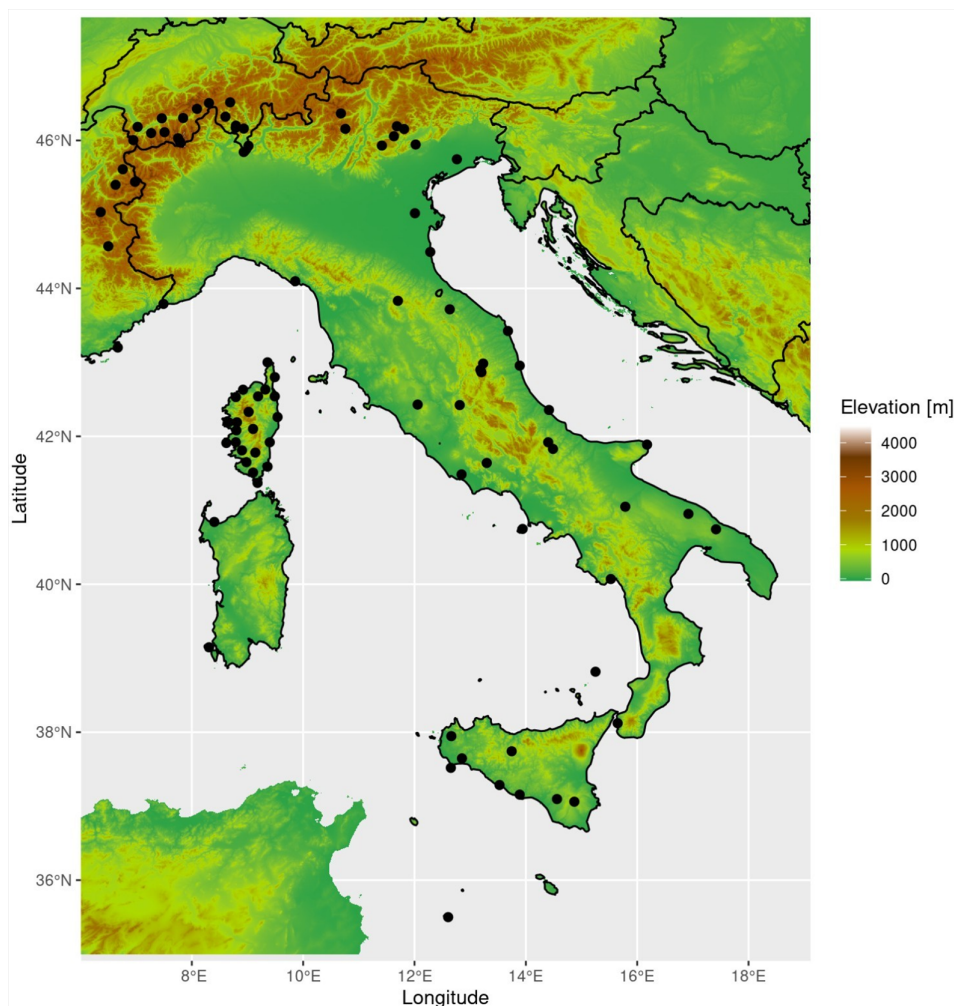
FIGURE 2 The 94 anemometer stations used for the 10-m wind validation.

and the impacts on the ground, for example, in hydrology, where the correct positioning of the rainfall structure plays a fundamental role in the streamflow response in a specific catchment of interest (Raimonet et al., 2017).

The gridded observational datasets used in the climatological comparisons for t2m and precipitation are provided by the University of Milan and ISAC-CNR (hereafter referred to as UniMi/ISAC-CNR) (Brunetti et al., 2012; Brunetti et al., 2014) on a 30 arc-seconds resolution grid ($\sim$ 1 km), using weather station observations available over Italy (merging the ARPA network with the Italian Air Force and Ente Nazionale Assistenza al Volo—ENAV—stations) and over neighboring countries (Meteo Swiss and the HISTALP dataset (Auer et al., 2007)) to cover the areas across the northern alpine border. The methodology used to interpolate the measured observations (both precipitation and t2m) into the 30 arc-second grid is based on the anomaly method described in Mitchell & Jones, 2005.

Specifically, this methodology enables the reconstruction of monthly temperature and precipitation fields by combining climatological values (long-term averages over

a specific reference period) with anomalies (deviations from these averages). For the t2m observational dataset, the approach follows the methodology outlined in Brunetti et al. (2014) and is applied in this study as described in Cavalleri et al. (2024). A similar process is used for precipitation.

Climatologies for both variables are derived from observations at all available stations—approximately 6000 for rainfall and around 1500 for temperature. These values are interpolated over a grid using locally weighted linear regression, taking into account station elevation and the spatial similarities between the grid cells and nearby stations in terms of horizontal and vertical distances, slope gradient, orientation, and distance from the sea (Crespi et al., 2018).

Anomalies are computed from a subset of stations used for climatologies, with only those having long-term records between 2000 and 2020 considered (<3000 for precipitation and <1000 for temperature). The anomaly fields are obtained from nearby stations using a combination of radial, vertical, and angular weighting functions to account for the uneven station distribution around each grid point (González-Hidalgo et al., 2011).

3 | RESULTS

3.1 | Multiyear evaluation

3.1.1 | Temperature

T2m climatological analyses were performed over the period 2000–2020, both in terms of climatological averages and daily deviations from climatology (i.e., anomalies), comparing MERIDA HRES (described in Section 2.1), MERIDA, and their driver ERA5 with the gridded observational maps provided by UniMi/ISAC-CNR (described in Section 2.2.2). Each reanalysis product was validated against gridded observations at the same native resolution of the reanalyses, without additional interpolations or upscaling, to minimize the influence of possible biases arising from different orographic representations (Luo et al., 2019).

From 2000 to 2020, climatologies (Figure 3) and t2m biases (Figure 3C) are obtained as the difference between each reanalysis product (Figure 3A) and the observations (Figure 3B).

The results show that the driver ERA5 exhibits cold biases of approximately −1°C across almost the entire Italian territory, except over the Po Valley, where there is a warm bias of approximately +0.5°C. MERIDA underlines a similar pattern in terms of cold and warm biases with some local intensifications of cold biases over the islands of Sicily and Sardinia and over the Alps, with more intense warm biases across the Alps foothills and the Po Valley. MERIDA HRES, in contrast, indicates a more uniform cold bias across all Italy.

At the seasonal level, spatially averaged bias values were obtained for the winter (DJF), spring (MAM), summer (JJA), and autumn (SON) (Table 2). MERIDA HRES exhibits the highest cold bias among the analyzed products for all the seasons, with a constant underestimation of approximately −1.4°C in all the seasons. The cold bias is a well-known characteristic of MERIDA HRES, probably due to the chosen PBL parameterization. Unlike the previous MERIDA reanalysis, the PBL was changed to enhance wind speed estimates using the topo_wind parameterization (as described in Section 2.1), which in WRF is incompatible with the same PBL used in the MERIDA reanalysis (MYJ—Mellor-Yamada-Janjic).

MERIDA tends to underestimate temperature as well, but with a more pronounced underestimation in summer. ERA5, on average, presents the best scores in terms of climatological biases for all the seasons, even if underestimating, as well. This does not necessarily imply that ERA5 is able to reproduce t2m fields better than MERIDA and MERIDA-HRES: the regional products, in fact, are better able to represent small-scale features and climate variability in complex terrain, with only slightly

greater deviations from observations than ERA5. The seasonal MAE was also calculated, confirming similar findings to those already highlighted with the bias analyses (and for these reasons, not shown).

The correlations between the t2m daily anomalies from the reanalysis and from the observations (Figure 4) show low values for all the reanalyses over Sardinia Island and over the coast of Sicily. In the Alps, ERA5 has the worst correlation values (below 0.9), whereas MERIDA has the highest correlation values across the entire alpine region. MERIDA HRES highlights a low-correlation area over the northwestern part of Italy (over the Alps, Po valley and coast) and a relatively better performance over the eastern part of the Alps and Po Valley. Seasonally, anomaly correlations are very high for all products and for all seasons and are all able to reproduce daily variability from climatology.

For comparison at the station level, we used the observational dataset of the ARPA network, which, for temperature, consists of approximately 2000 thermometers. The reanalysis data have been bilinearly interpolated in correspondence with the stations, choosing a neighborhood of four grid points from the thermometer location. In this verification, we did not apply a correction between the model grid points and the station to follow the same approach used in Bonanno et al. (2019). Statistics are calculated in terms of bias and RMSE for the period 2016–2020 and are averaged over the whole domain as a function of the time of day, as shown in Figure 5.

Compared with ERA5, MERIDA has a similar bias but a lower error for almost all hours. MERIDA HRES suffers from a cold bias already noted by the previous analysis on gridded data, which slightly degrades its performance, resulting in a bias between −0.5 and −1°C. However, its error is still lower than that of ERA5 and comparable to that of MERIDA in some hours, especially in the first hours of the morning. The same indices calculated as an average over the months shown in Figure 6 describe a similar situation, with MERIDA HRES showing higher negative bias.

Figure 7 shows the maps of bias computed for each station and model. Overall, MERIDA shows slightly better results than the other models do, even if it follows a very similar pattern of cold and warm bias to that of ERA5. MERIDA HRES, in contrast, confirms a general cold bias in most of the peninsula, which is also observed in the gridded analyses, even if it produces some small warm bias over the Po Valley and the coasts. Compared with MERIDA and ERA5, MERIDA HRES also generally has greater negative biases on complex terrain.

Overall, the temperature analyses highlight the tendency of all the reanalysis products to underestimate t2m. Most likely, because ERA5, the driver, produces a
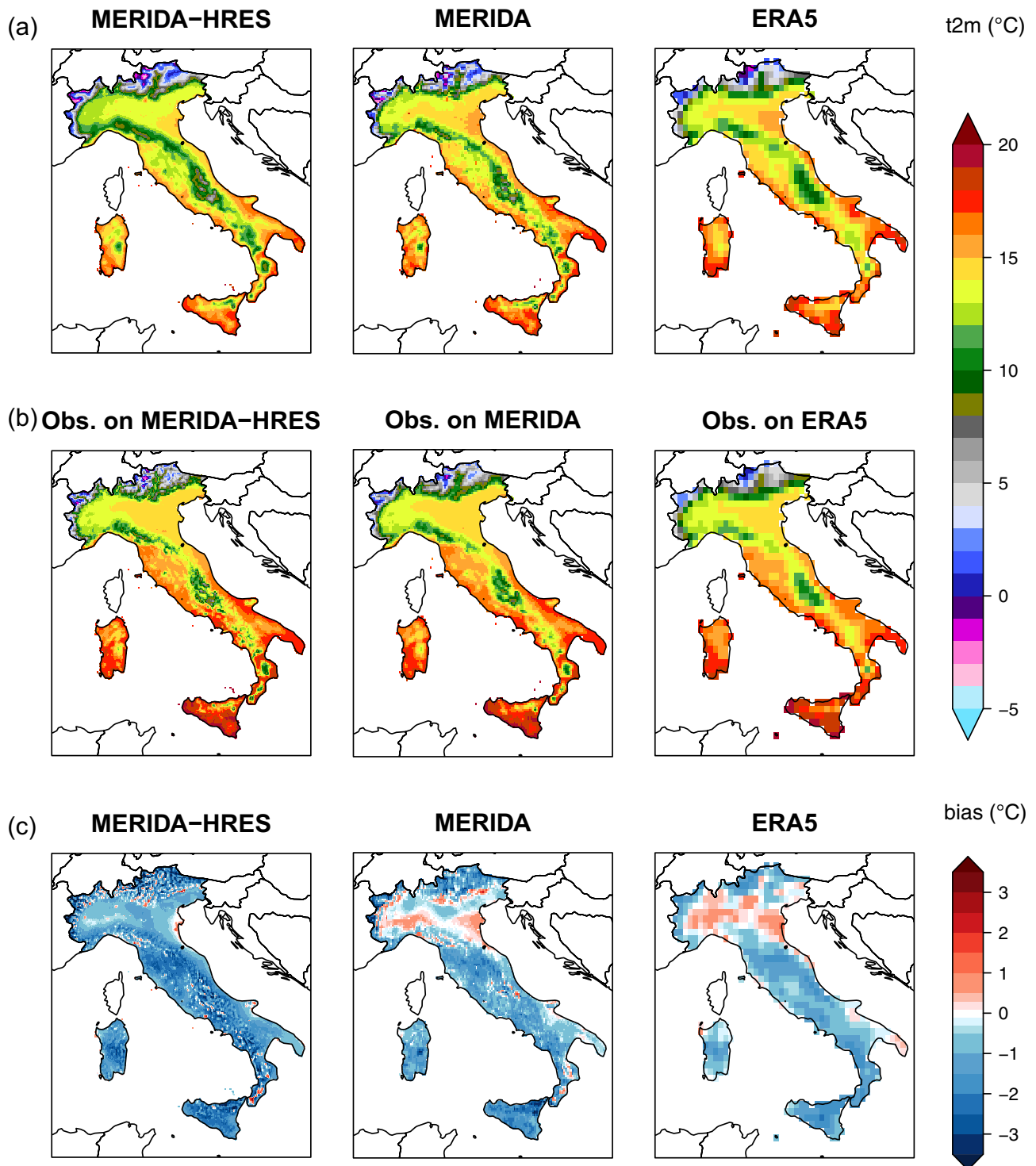
FIGURE 3 Climatology from the reanalyses (a) and gridded observational dataset (b) for the period 2000–2020 for the MERIDA HRES (column 1), MERIDA (column 2), and ERA5 (column 3) datasets. (c) represents the t2m bias against observations for MERIDA HRES (column 1), MERIDA (column 2), and ERA5 (column 3).

cold bias, the regional reanalyses also tend to inherit this tendency, as proven, for example, by the very similar temperature patterns (and, consequently, biases) between ERA5 and MERIDA (Figures 3 and 7). Nevertheless, MERIDA HRES tends to amplify this behavior, especially

over orography, showing a systematic cold bias of at least −1°C in all the analyses performed across seasons (Table 2), hours of the day (Figure 5), and months of the year (Figure 6), both for station and gridded datasets, even if slight differences in the magnitude of the bias

TABLE 2 Seasonal t2m statistics (bias and correlation) for climatological values and anomalies for the reanalysis (MERIDA HRES, MERIDA, and ERA5) and gridded UniMi/ISAC-CNR observations.

			MERIDA HRES	MERIDA	ERA5
Climatological deviations	Average Bias (°C)	DJF	−1.49	−0.77	−0.67
		MAM	−1.41	−0.35	−0.69
		JJA	−1.45	−1.26	−0.60
		SON	−1.39	−0.89	−0.56
		Yearly	−1.40	−0.81	−0.63
Anomalies	Correlation	DJF	0.93	0.95	0.93
		MAM	0.95	0.95	0.95
		JJA	0.95	0.96	0.95
		SON	0.94	0.95	0.94
		Yearly	0.94	0.95	0.94

exist, owing to the different natures of the ground-truth analyzed. On the other hand, MERIDA HRES is still able to reproduce the temporal variability in temperature, even if not the absolute value, as proven in temperature anomaly analyses (Figure 4 and Table 2).

3.1.2 | Precipitation

We assessed MERIDA HRES precipitation fields with ERA5 and MERIDA against both gridded (UniMi/ISAC-CNR) and station-based (from the ARPA stations) observational datasets.

First, the 2000–2020 climatological average of total annual precipitation (Figure 8) was computed, and similar climatological values and patterns were obtained for the MERIDA HRES, MERIDA, and ERA5 datasets, even with different degrees of detail due to the different native resolutions.

However, to ensure a fair comparison, we conservatively upscaled the MERIDA HRES and MERIDA fields to the coarser resolution of ERA5 to calculate the relative biases against the UniMi/ISAC-CNR gridded observations (Equation 1). In Equation 1, tp_{rean} represents the climatological total precipitation average from the reanalysis, while tp_{obs} is the corresponding observational value.

$$\%\text{bias} = \frac{(tp_{\text{rean}} - tp_{\text{obs}})}{tp_{\text{obs}}} \qquad (1)$$

The relative bias was chosen to account for the strong seasonal variability in the magnitude of precipitation, which can negatively affect the quantification of bias in the months with the highest seasonal precipitation amounts (Tian et al., 2013).

From the relative bias maps (Figure 9), the MERIDA HRES reanalysis exhibits a similar pattern to those of the MERIDA and ERA5 reanalyses, even with smaller and less spatially extended relative bias values. Specifically, MERIDA HRES does not exhibit the pronounced wet biases in the western Alps and Po Valley observed in ERA5, nor does it display the strong dry biases observed by MERIDA along the southern Apennines and Sicily.

Compared with those of ERA5 and MERIDA, the spatial averages at the seasonal scale (Table 3, upper rows) confirm the best performance of MERIDA HRES for all the seasons, with relative biases lower than 5% in all the seasons except summer. In summer (JJA), all the reanalyses show the highest biases, probably because of the known difficulties of both models and observations in depicting summer convection storms (Weisman et al., 1997). Nevertheless, among all the products, the MERIDA HRES exhibits the lowest precipitation bias (+20%) in summer, probably because it explicitly solves convection without using parameterizations, such as ERA5 and MERIDA.

Although upscaling the gridded analyses to match the coarsest ERA-5 resolution allows for a fairer comparison in the calculation of the relative bias, it is important to emphasize that upscaling high-resolution models to a coarser resolution may obscure potential errors at finer local scales. Although specific scale-separation diagnostics are reserved for a future and more specific study, station verifications are here used to help evaluate reanalyses performance at finer scales by comparing reanalyses at native resolution with station observations.

In addition to gridded verification, we computed the Stable Equitable Error in Probability Space (SEEPS) (Haiden et al., 2012) (Rodwell et al., 2010) via a subset of the ARPA rain gauges (described in Section 2.2.1), which were measured for at least 25% of the days in the
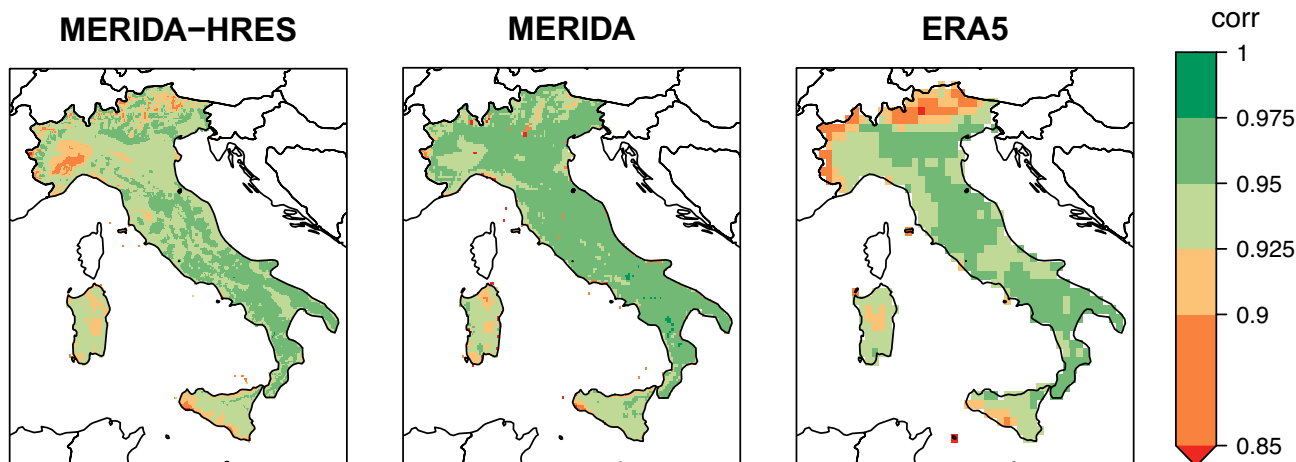
FIGURE 4 Climatological correlation between reanalysis and observational t2m daily anomalies for ERA5, MERIDA, and MERIDA HRES for the period 2000–2020.
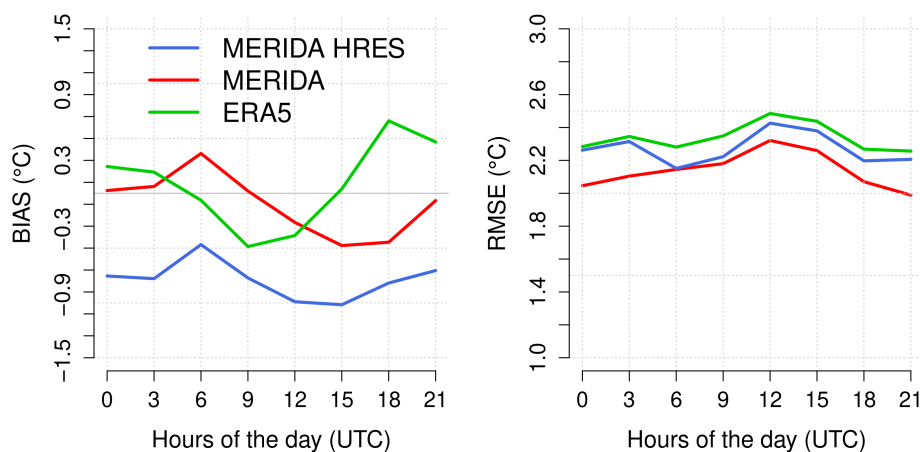

FIGURE 5 Bias (left) and RMSE (right) as a function of the time of day computed over the available stations over the 2016–2020 period. Comparison between MERIDA HRES (blue), MERIDA (red), and ERA5 (green).

2016–2020 period and for all the seasons. The number of valid stations once applied this condition is 1622 for the annual analysis and 1625, 2052, 2159, and 2141 for winter (DJF), spring (MAM), summer (JJA), and autumn (SON), respectively. SEEPS classify precipitation into 'dry days', 'light precipitation', and 'heavy precipitation' via a categorical approach that penalizes fewer multiplicative errors that can typically arise in precipitation evaluation (Tian et al., 2013). In this approach, 'dry days' are defined as days with accumulated precipitation less than 1 mm in 24 h. Stations with a probability of occurrence of dry days (p_1) less than 10% of the time or more than 85% of the time (i.e., stations with $0.1 < p_1 < 0.85$) are not used in the SEEPS calculation, as they do not provide an adequate sample of diverse precipitation categories. The 'light precipitation' and 'heavy precipitation' days in SEEPS are based on the 2016–2020 climatology, ensuring that light precipitation occurs twice as frequently as heavy precipitation (Haiden et al., 2012). SEEPS is calculated as 1 minus the scalar product between the

contingency matrix (reanalysis rainfall categories against observed rainfall categories) and the S matrix (see Equation 2), as defined by Haiden et al. (2012). SEEPS varies from 1 to 0, where 1 is a 'perfect score' and 0 is an 'unskilled product'.

$$S = \frac{1}{2} \begin{pmatrix} 0 & \dfrac{1}{1-p_1} & \dfrac{4}{1-p_1} \\ \dfrac{1}{p_1} & 0 & \dfrac{3}{1-p_1} \\ \dfrac{1}{p_1} + \dfrac{3}{2+p_1} & \dfrac{3}{2+p_1} & 0 \end{pmatrix} \qquad (2)$$

The average SEEPS scores for each station over the 2016–2020 period (Figure 10) show the worst performance for MERIDA, especially in the Apennine region and over Sicily and Sardinia islands.

ERA5 and MERIDA HRES both demonstrate very good performance, even if the high resolution of

FIGURE 6 Bias (left) and RMSE (right) as a function of the month computed over the available stations over the 2016–2020 period. Comparison between MERIDA (red), MERIDA HRES (blue), and ERA5 (green).
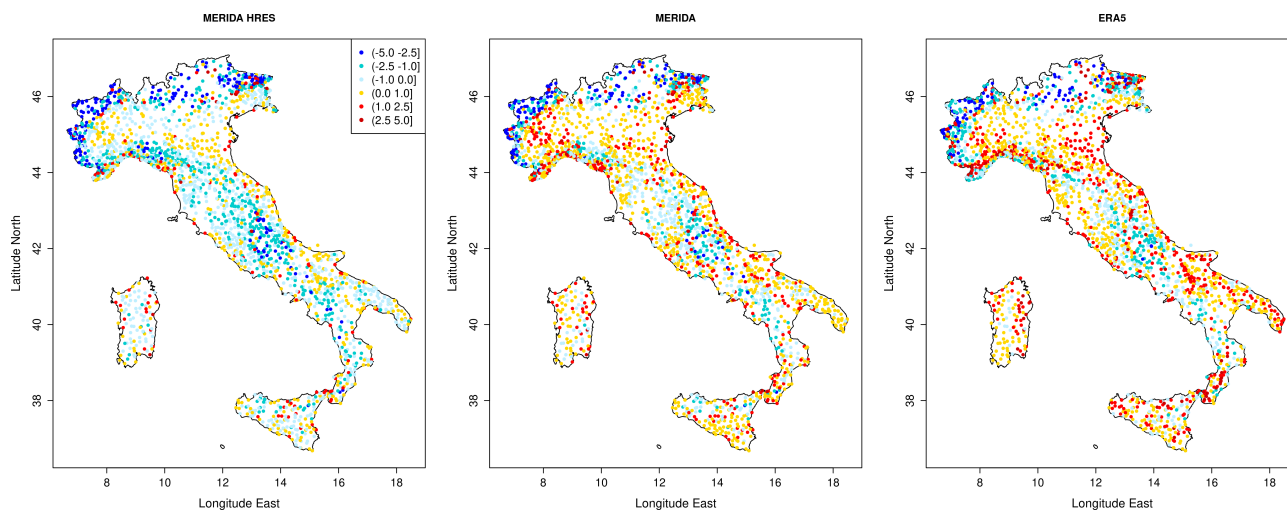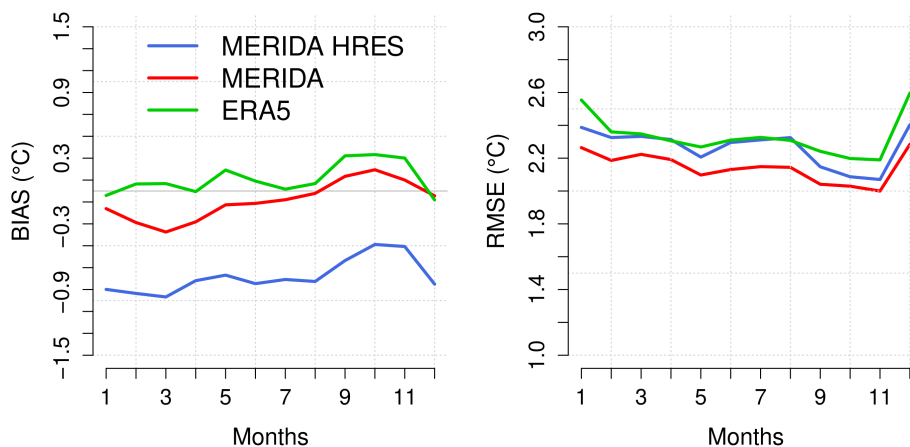

FIGURE 7 Maps of t2m bias computed for the available stations and for each model over the 2016–2020 period. From left to right: MERIDA HRES, MERIDA, and ERA5.

MERIDA HRES might be more penalizing than the coarse resolution ERA5, in accounting for the risk of double penalties (Jermey & Renshaw, 2016) in point station verification. Seasonal evaluation (Table 3, lower rows) confirms that MERIDA HRES consistently produces higher SEEPS values than MERIDA, which is indicative of its superior capacity to discriminate between dry days, light, and heavy precipitation. Moreover, its ability to achieve SEEPS values is comparable to that of ERA5, despite operating at a significantly (more challenging) higher resolution, suggesting even greater effectiveness in accurately depicting precipitation patterns.

To account for possible precipitation displacement and, consequently, the risk of 'double penalties', a fuzzy verification procedure (Ebert, 2008) was also applied through contingency table evaluations (Table 4) via ARPA raingauges.

The fuzzy procedure (Ebert, 2008) is based on aggregating rain gauges in regular boxes of approximately

40 km, considering only those with at least five stations with available and valid data for the considered period. This avoids the problem of penalizing high-resolution simulations due to small displacement errors, which results in doubling the penalty effect so that increasing the resolution might decrease the score (Lanciani et al., 2008).

Precipitation is verified using the Hanssen and Kuipers score (HK) (Hanssen & Kuipers, 1965) (Equation 3), which is positively oriented (i.e., perfect score: 1). It consists of the difference between the hit rate (HR), also known as the probability of detection (POD), and the false alarm ratio (FAR) calculated for different thresholds from the contingency table (Table 4). The HR (perfect score: 1) and FAR (perfect score: 0) are defined in Equations 4 and 5.
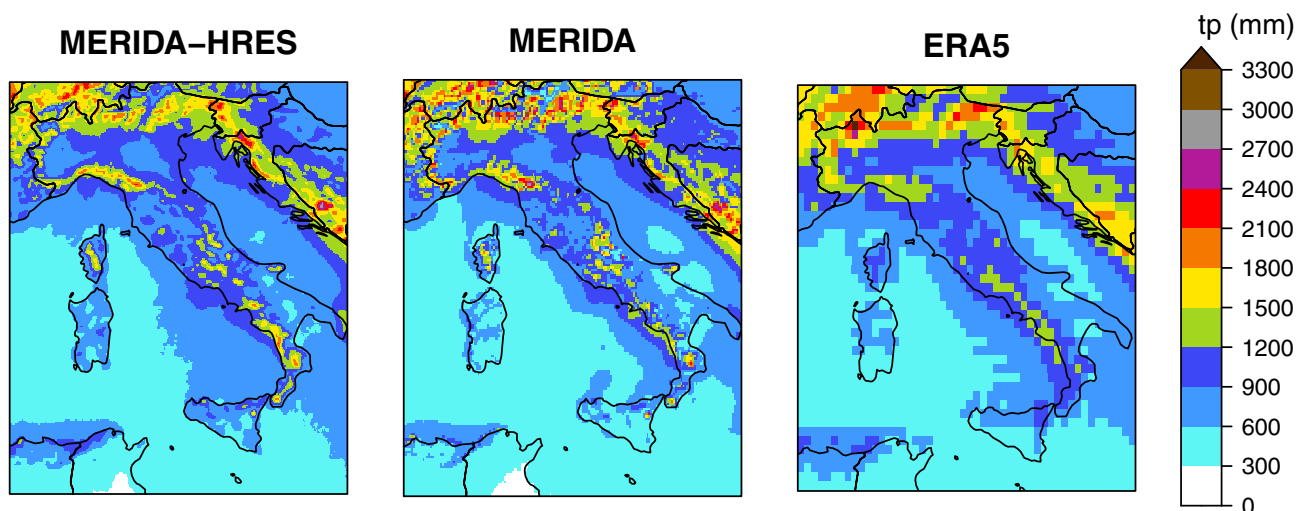
$$HK = HR - FAR \qquad (3)$$

FIGURE 8   Climatological 2000–2020 averages of the annual precipitation at the native resolution of the MERIDA HRES, MERIDA, and ERA5 datasets.
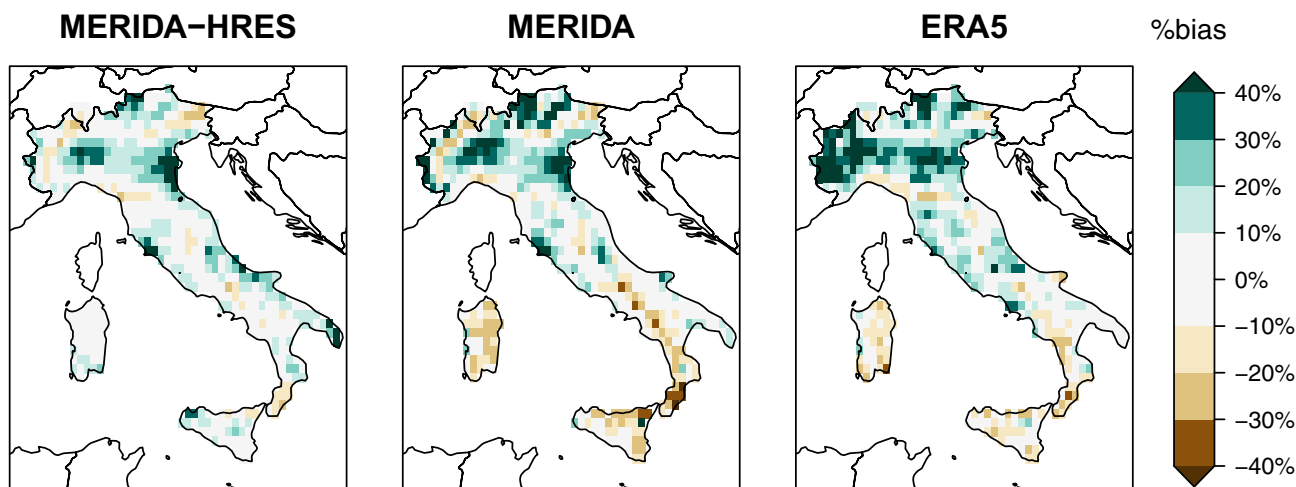

FIGURE 9   Climatological (2000–2020) annual relative precipitation bias against gridded observations (UniMi/ISAC-CNR) for MERIDA HRES, MERIDA, and ERA5 (from left to right).

$$HR = \frac{hits}{hits + misses} \qquad (4)$$

$$FAR = \frac{false\ alarms}{false\ alarms + correct\ negatives} \qquad (5)$$

The HK and FAR are calculated for daily precipitation thresholds from 10 to 100 mm with 10 mm bins (Figure 11). The indices are calculated on the 95th percentile (p95) of the cumulative daily precipitation data inside each 40 × 40 km box, making it possible to evaluate the model performance considering the daily peak, which is relevant for identifying weather extremes to locate strong precipitation events.

The HK of MERIDA has lower (i.e., worse) values, which are paired with lower (i.e., better) FAR values. This is due to its lower horizontal resolution, which tends to homogenize the values inside the boxes. The higher resolution datasets have additional value and are able to capture the precipitation peaks inside the 40-km boxes, especially MERIDA HRES (which has a better HK but a slightly worse FAR than MERIDA).

Additional verification is carried out via the Performance Diagram (Roebber, 2009) (Figure 12), which provides a summary of the reanalysis performances obtained by combining the HR (y-axis) with three additional indices that can be obtained from the contingency table: Success Ratio (SR, x-axis, Equation 6), frequency bias (dashed line with labels on the outward extension of the

TABLE 3 Seasonal and yearly spatially averaged scores for MERIDA HRES, MERIDA, and ERA5.

		MERIDA HRES	MERIDA	ERA5
Relative Bias (period 2000–2020)	DJF	2%	−13%	0%
	MAM	4%	11%	14%
	JJA	20%	46%	23%
	SON	3%	−8%	4%
	Yearly	7%	9%	10%
SEEPS (period 2016–2020)	DJF	0.69	0.59	0.67
	MAM	0.62	0.58	0.65
	JJA	0.43	0.41	0.49
	SON	0.63	0.55	0.65
	Yearly	0.61	0.55	0.64
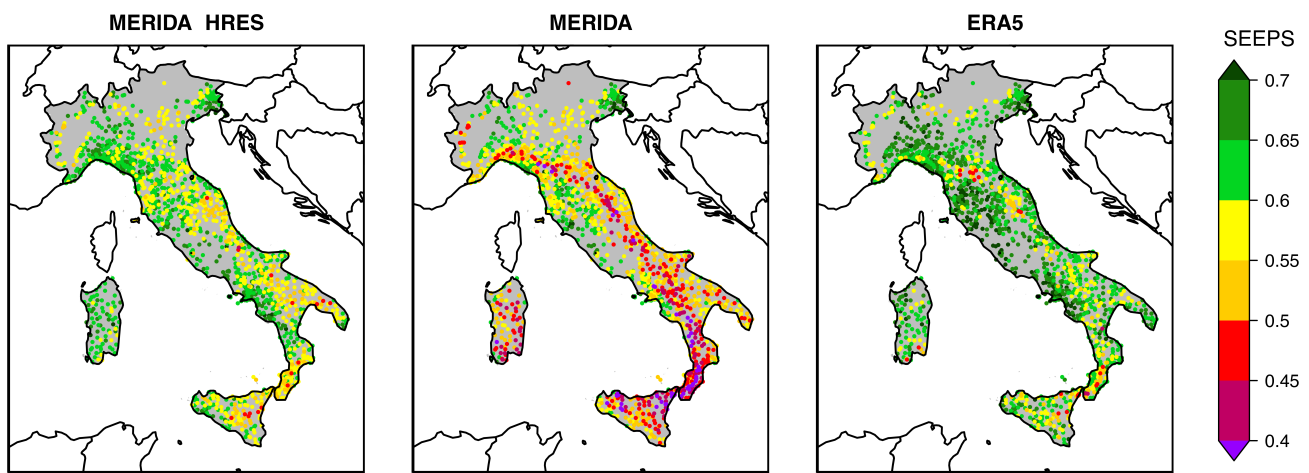
FIGURE 10 Daily SEEPS skill scores averaged over the period 2016–2020 for MERIDA-HRES, MERIDA, and ERA5 (from left to right) against ARPA raingauges.

line, Equation 7) and Critical Success Index (CSI, solid contour, Equation 8). The scores are calculated using the same thresholds as in the previous HK verification (from 1 to 100 mm/day, with 10 mm intervals). Naturally, the sample size decreases at higher thresholds, as extreme precipitation events are less frequent. Consequently, at higher thresholds, the smaller sample size may introduce greater uncertainties in the results. Table S1 in the Supporting Information material provides the sample sizes for each threshold and dataset used in the comparison.

$$SR = \frac{hits}{hits + false\ alarms} \quad (6)$$

$$frequency\ bias = \frac{hits + false\ alarms}{hits + misses} \quad (7)$$

$$CSI = \frac{hits}{hits + misses + false\ alarms} \quad (8)$$

As is likely already evident, in this case, the frequency bias used in the performance diagram (and represented in Equation 7) differs from the common deviation between the modeled and measured data, as described in Section 2.1. The best performance is given by all indices tending to 1, that is, on the 1:1 line on the upper right corner of the diagram. Model accuracy increases when moving on the 1:1 line, thus maintaining zero frequency bias and increasing the correct detection of events, thus reducing false positives. The diagram also allows us to consider the influence of sampling variability, using a bootstrap of data and plotting the confidence intervals for the SR and POD as lines perpendicular to the axes, in correspondence with the various models.

The diagram reflects the results of Figure 11 while providing additional information about the ability of each model to depict different precipitation intensities at the daily scale. For the higher thresholds (i.e., above 50 mm/24 h), MERIDA HRES appears to be the best

model, lying more toward the 1:1 line than the other models do, due to its higher horizontal resolution, which allows more correctly intense precipitation events to be captured (Figure 12).

TABLE 4 Contingency table.

		Observed	
		Yes	**No**
Modeled	Yes	Hits	False alarms
	No	Misses	Correct negatives

Overall, all the precipitation analyses revealed the superior ability of the MERIDA HRES to depict precipitation, especially extreme values, compared with MERIDA (Figures 11 and 12). MERIDA shows the highest errors over the orography, especially over the Apennines (Figures 9 and 10). Without accounting for double-penalty errors, MERIDA HRES and ERA5 have similar performances (Figure 10 and Table 3), whereas when fuzzy verification techniques are used for a fairer comparison for high-resolution reanalyses, MERIDA HRES results in the best performance compared with the other products, especially for thresholds higher than
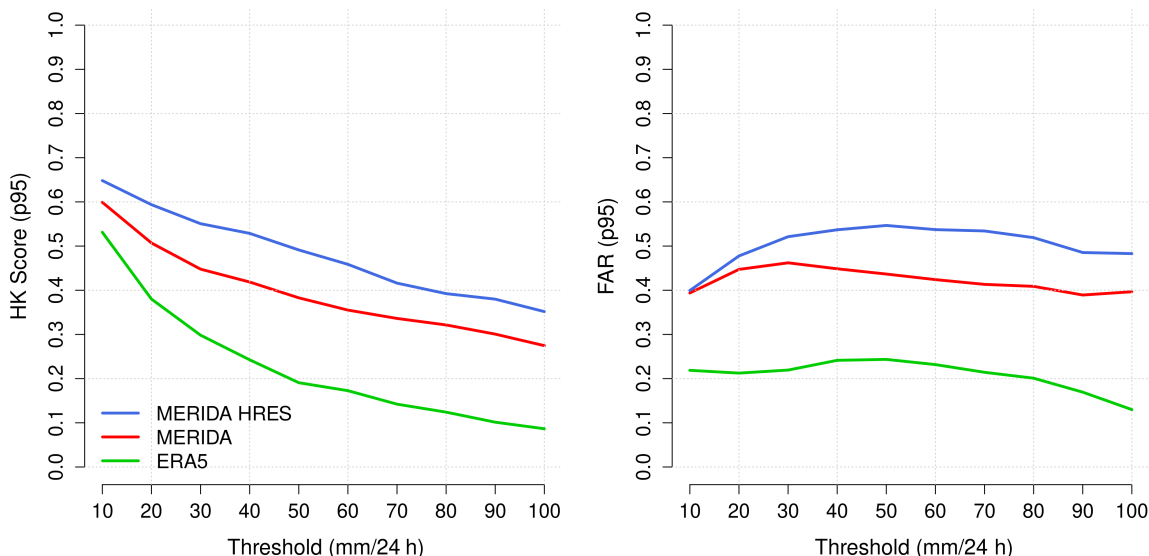

FIGURE 11 HK score (left) and FAR (right) on the p95 of the cumulative daily precipitation data as a function of thresholds (from 1 to 100 mm/day with 10 mm bins) computed over the available ARPA rain gauge stations and the 2016–2020 period.
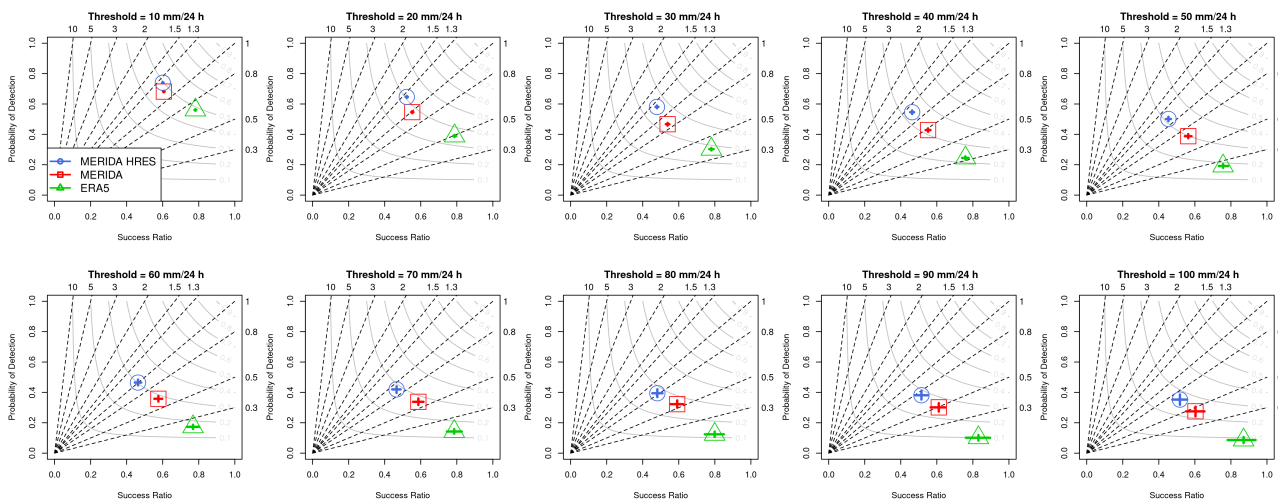

FIGURE 12 Performance diagram for the p95 of the cumulative daily precipitation data computed over the available stations and the 2016–2020 period for different threshold values (from 1 to 100 mm/day with 10 mm bins). Comparison of MERIDA HRES (blue circles), MERIDA (red squares), and ERA5 (green triangles).

50 mm/day (Figures 11 and 12). As expected, all the reanalysis products present greater difficulties in reproducing summer precipitation due to convection, whereas the MERIDA HRES 4-km resolution and explicit convection result in an advantage in obtaining the best results in summer compared with the other products (Table 3).

3.1.3 | Wind speed

The 10-m wind verification follows a similar approach to that in Sperati et al. (2024), using the same set of 94 observational stations, as shown in Figure 1, Section 2.2.1.

The biases of MERIDA HRES, MERIDA, and ERA5 are assessed by comparing their wind values to station observations, with a focus on evaluating potential improvements in reconstructing 10-m winds using configurations different from those of MERIDA. This approach is consistent with the original purpose behind the design of MERIDA HRES (explained in greater detail in Section 2.1). The nearest model grid point to each station was used, and bias was calculated as a function of the station's terrain elevation (Figure 13), where terrain elevation is derived from the orography of each reanalysis model. When multiple stations fall within the same reanalysis grid box, the wind value from the reanalysis model is compared individually with each station, while the model's elevation remains constant for all stations within that grid box.

Because of the sometimes-poor availability of measured data, in this case, each station has a different length of the evaluation period, selecting the maximum available length for the verification time series, with a minimum requirement of at least 2 years of continuous records in the period 2010–2020 for each station.

The results show that MERIDA HRES can lower the bias of MERIDA, keeping it below 1 m/s for most of the stations (Figure 13). ERA5 shows a rapidly increasing bias with terrain elevation due to its lower horizontal resolution and subsequent limited ability to reproduce the orographic complexity that affects the wind field. The positive bias of both MERIDA and MERIDA HRES is noticeable at approximately 0 m asl, which probably refers to stations close to the shore, where some errors in representing the land–sea interface by WRF are common (Sperati et al., 2024).

Additional analyses are carried out to study how the reanalyses reconstruct the wind speed distributions using the Kolmogorov–Smirnov (KS) (Wayne, Wayne, 1990) index (Equation 9, where f_s and f_o are the simulated and observed probability distributions, respectively), which quantifies the maximum differences between the cumulative frequency distributions, thus providing a measure of the similarity between two distributions without making assumptions on the shape of the distribution. The KS index is calculated using a bin size of 0.5 m/s, and it is negatively oriented (i.e., the lower the score is, the better the performance).

$$KS = \left| \max_x \left(\int_{-\infty}^{x} dx' f_s(x') - \int_{-\infty}^{x} dx' f_o(x') \right) \right| \quad (9)$$

The KS, expressed as a function of terrain elevation (Figure 14), shows a slightly better reconstruction of the wind distribution by MERIDA HRES than MERIDA, with a lower KS at most of the stations. ERA5 shows
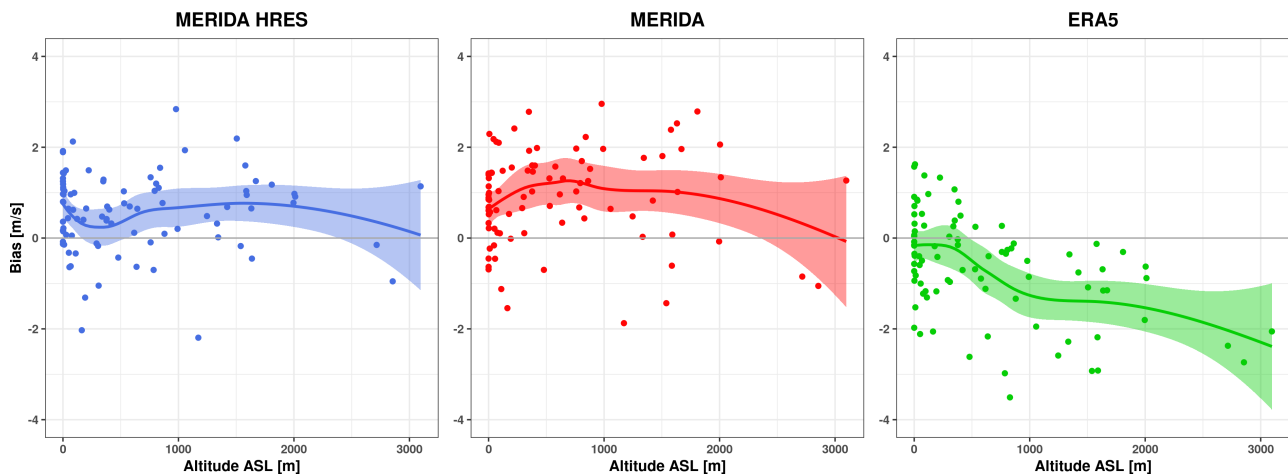

FIGURE 13   Bias as a function of the terrain elevation of each station. Comparison between MERIDA HRES (left), MERIDA (center) and ERA5 (right) in periods with available data. Data are extracted via nearest neighbor interpolation corresponding to each of the 94 observational anemometer stations. The curves are defined using locally estimated scatterplot smoothing (LOESS) regression (Cleveland et al., 1992).
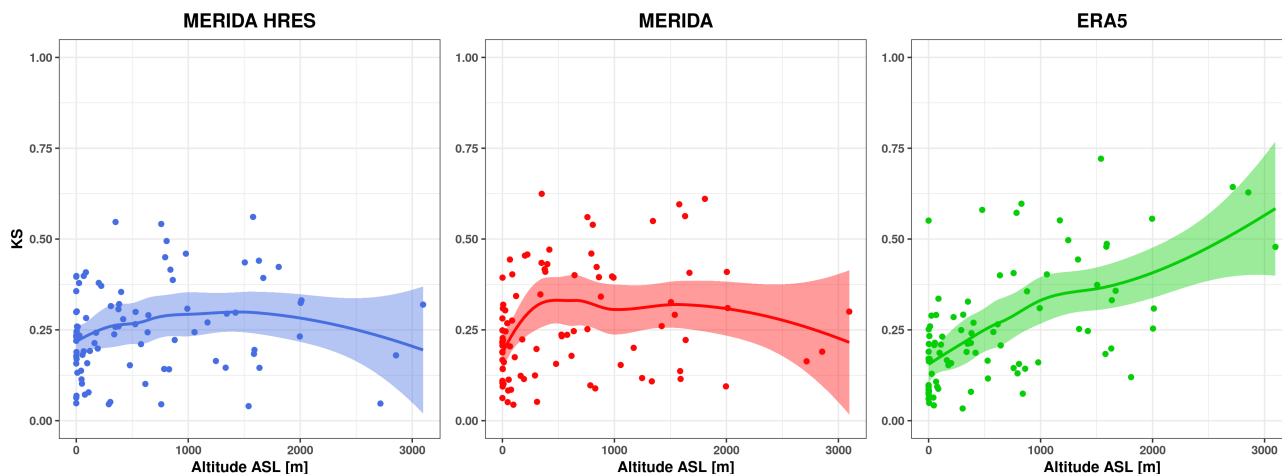
FIGURE 14 KS as a function of terrain elevation, comparison between MERIDA HRES (left), MERIDA (center), and ERA5 (right). The data are extracted via nearest neighbor interpolation in correspondence with the 94 observational stations. The curves are defined using locally estimated scatterplot smoothing (LOESS) regression (Cleveland et al., 1992).

good KS values at lower terrain elevations, but it progressively worsens as the orographic complexity increases.

3.2 | Extreme events analyses

The main purpose of this paper is to provide a complete picture of the strengths and weaknesses of the newly developed MERIDA HRES reanalysis product over Italy and to promote awareness of the use of these reanalyses for scientists and stakeholders for multiple applications in different fields, from the atmospheric sciences to the energy sector. For these reasons, this part of the paper is meant to showcase the possible applications and the information that can be derived from the MERIDA HRES reanalysis regarding its ability to model extreme events.

In particular, to provide a fair assessment of the capabilities of MERIDA HRES across multiple kinds of extreme events and variables of interest, a very diverse set of events at different scales are presented: (i) an intense convective precipitation event, which occurred in the area of Bergamo (northern Italy, foothills of the central sector of the alpine region) during the summer of the 31 July 2016; (ii) a more synoptically driven storm, known as the Vaia storm, which produced precipitation and very strong winds over the eastern Alps at the end of October 2018; and (iii) a wildfire event that occurred in 2017 in Sardinia (known as the Arbus fire).

Additionally, most of these events happened in complex orography areas, which is an additional reason for evaluating the performance of 4-km reanalyses with explicit convection, such as MERIDA HRES, compared with its predecessor MERIDA and its driver ERA5 to investigate its potential added value.

3.2.1 | Convective precipitation event over Bergamo on 31 July 2016

On the morning of 31 July, 2016, a convective multicell system swept the center-north part of the Po valley, producing intense precipitation (locally over 100 mm/24 h) and a gust front moving eastward close to the (alpine) foothill line, causing black-out in the area for several hours, with many reports of fallen trees over roads and infrastructure and interruptions to trains and road traffic.

We expect MERIDA HRES to better represent the precipitation pattern and timing of such an event than MERIDA because of its higher resolution and updated PBL parameterizations. We compared modeled 24-h accumulated precipitation (MERIDA HRES, MERIDA and ERA5) with gridded and point observations from the ARCIS dataset (Isotta et al., 2014) and from rain gauge data from regional environmental protection agencies (ARPAs), such as those used in the previous analyses and described in Section 2.2.1.

As shown in Figure 15, the daily accumulated rainfall map produced by MERIDA HRES exhibits significantly better agreement with the observations than those produced by MERIDA and ERA5, both in terms of maximum values and spatial distribution, even with a minor displacement of the precipitation peak (approximately 30-km westward).

The time series of two stations (named "Filago" and "Osnago") located in proximity to the observed maximum precipitation (Figure 16) confirm the good performance of MERIDA HRES in the timing of the event, despite a reasonable underestimation (<10 mm—20% for both locations) of the observed maximum. In particular, Figure 16 shows that MERIDA HRES locates the event
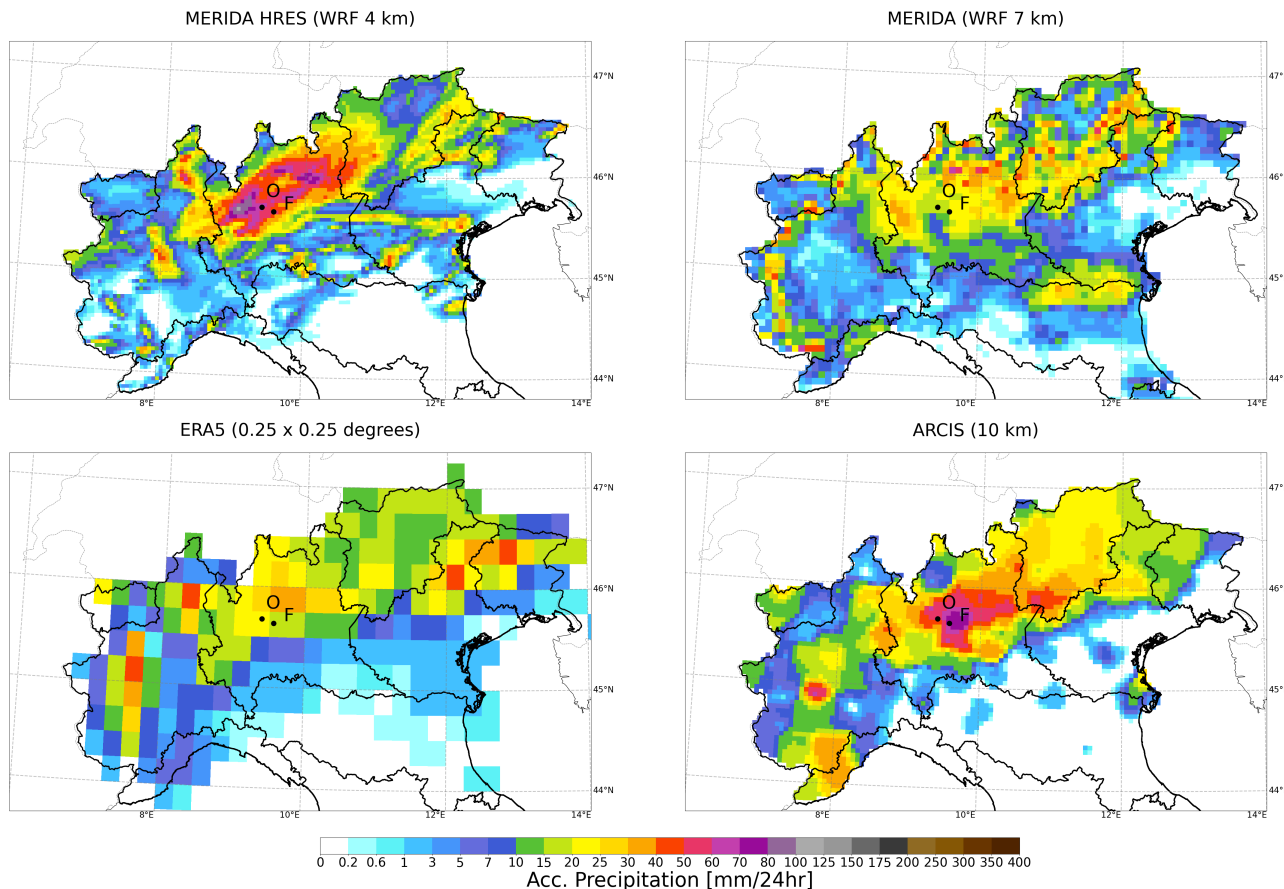
FIGURE 15 Daily accumulated precipitation maps (mm/24 h) for MERIDA HRES, MERIDA, ERA5, and ARCIS during 31 July 2016 convective precipitation event. The points indicated as "O" and "F" refer to the locations of the ARPA stations of Osnago and Filago, respectively (see Figure 16).
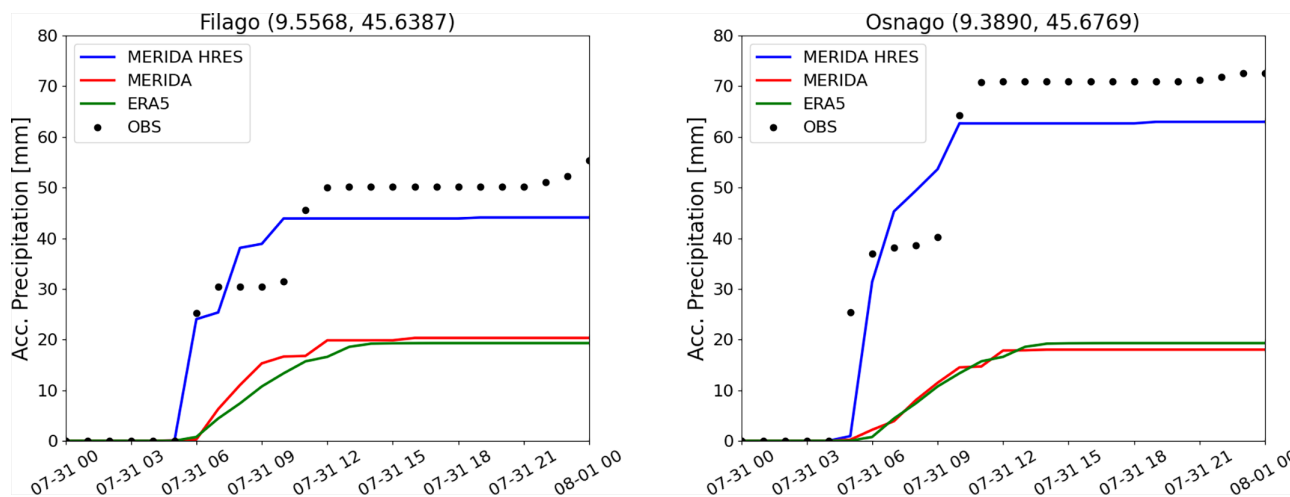

FIGURE 16 Time series of the accumulated precipitation during the 31st July 2016 event for the ARPA stations of Filago and Osnago.

during the few hours with the most intense observed precipitation (50 and 71 mm in 7 h, respectively, at Filago and Osnago), with a precise match in the starting time, whereas both MERIDA and ERA5 underestimate and distribute rainfall over a longer time span.

Consistent with the analysis reported in Section 3.1, this case study demonstrates the improved ability of MERIDA HRES compared with its predecessor MERIDA in reproducing convective precipitation events, which are based on kilometer-scale phenomena.

3.2.2 | The Vaia storm on 28 October–2 November 2016

Similar to the previous section, we compared the performance of MERIDA HRES with MERIDA in the context of the well-studied Vaia storm (Giovannini et al., 2021), which affected Italy between 28.10.2018 and 02.11.2018. The event was associated with a synoptic upper-level trough over the western Mediterranean, which drove strong moist southerly currents toward the Adriatic Sea and the Veneto region, causing exceptional precipitation and wind speeds and severe wooden forest destruction over the south-eastern alpine ridge. In this case, the ERA5 maps were not included in the comparison because of their evident inadequacy in reproducing the strong interactions of the wind with the complex orographic features of ridges and valleys due to their low horizontal resolution (∼31 km).

The advantage of HRES in modeling wind in complex terrain is linked to the advanced wind parameterization (topo_wind (Jimenez & Dudhia, 2012), see Section 2.1) and higher resolution (see Section 2.1 for a more detailed description of MERIDA HRES settings). As shown in Figure 17, the HRES wind distribution shows peaks over elevated areas and crests, which are more impacted by higher-level winds, whereas MERIDA struggles to accurately reproduce winds consistent with the region's orographic features and generally underestimates the maximum wind gusts. This is achieved despite the very similar model orography of the two models (as shown in Figure 17).

We investigated in greater depth two locations (Passo Manghen and Col della Gallina) affected by extreme winds during the Vaia storm. The observed wind speed is compared against model data extracted from grid cells corresponding to the horizontal position of the stations and, additionally, from neighboring cells. This is necessary because the model terrain (both MERIDA and MERIDA HRES) significantly locally underestimates the elevation (on the order of hundreds of meters, see Table 5), which may distort the results. To reduce this elevation gap and ensure a better representation of the orography, neighbouring cells are therefore selected following the maximum gradient of the terrain and within an area of ±2 grid cells. Locations with the best elevation matching are chosen.

The comparison is carried out through a statistical evaluation based on the root mean squared error (RMSE) and the average bias.

At Passo Manghen, MERIDA HRES shows greater variability than MERIDA (RMSE: 3.71 and 2.85 m/s, respectively) (Table 5), which is nevertheless linked to higher maxima (occurring over the night between the 27th and the 28th October and the afternoon of 29th October) (Figure 18), which are better captured by HRES in terms of intensity, despite a temporal shift of a few hours, which results in a lower negative bias for HRES (−0.61 m/s) compared with MERIDA (−1.28 m/s) (Table 5).

At Col della Gallina, a significant negative bias is found for MERIDA (−7.19 m/s) and for ERA5 (−8.29 m/s) (Table 5), whereas HRES is closer to observations
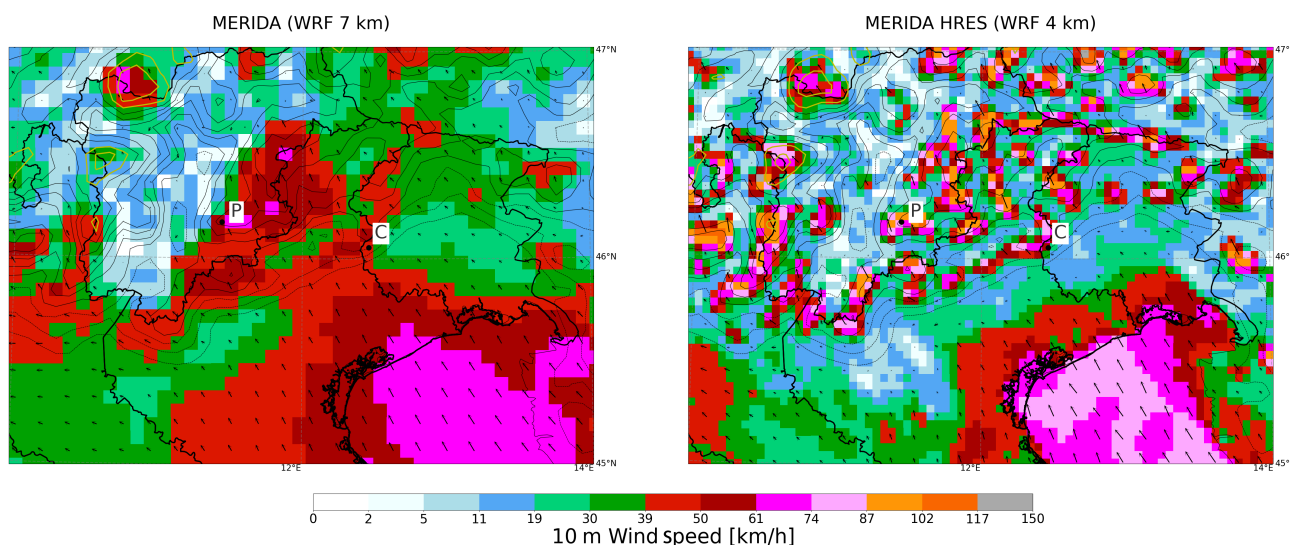

FIGURE 17 10-meter wind maps (km/h) for MERIDA and HRES at 2018.10.29 18:00 (ERA5 not shown here). The wind intensity is represented with the color palette, the wind speed and direction are indicated by oriented arrows, and the model terrain is shown as contour isolines with 250-m spacing (yellow lines indicate heights >2500 m). The points indicated as "P" and "C" refer to the ARPA stations of Passo Manghen and Col della Gallina, respectively (see Figure 18).

TABLE 5 Statistics of the comparison between the models and observations during the Vaia storm event for the Passo Manghen and Col della Gallina stations. *MERIDA HRES* refers to* a point that is one grid cell east (+1x) and two cells north (+2y) of the original cell for Passo Manghen and Col della Gallina, respectively.

Model		MERIDA HRES	MERIDA HRES*	MERIDA	ERA5
Passo Manghen (2035 m a.s.l.)	RMSE (m s^{-1})	3.71	3.43	2.85	8.68
	Bias (m s^{-1})	−0.61	−1.32	−1.28	−7.84
	Model elevation (m a.s.l.)	1782	1826	1810	1433
Col della Gallina (1336 m a.s.l.)	RMSE (m s^{-1})	5.75	4.17	7.19	9.46
	Bias (m s^{-1})	−4.23	−1.73	−6.18	−8.29
	Model elevation (m a.s.l.)	885	1144	781	289

(−4.24 m/s) (Table 5), especially for the most intense phases (Figure 18). Due to the large elevation discrepancy between the model elevation and the actual elevation for this station (see Table 5), more reasonable results are found for HRES* (2 grid cells northward, 1134 m), which shows a smaller bias (−1.73 m/s) and RMSE (4.17 m/s), together with a very good representation of the peak intensity and timing (Figure 18).

On the other hand, at Passo Manghen, the chosen neighboring cell (1 cell eastward, 1826 m a.s.l.) shows a limited improvement, likely due to a small elevation gap reduction. Additionally, we highlight that very small changes are found if one selects neighboring cells for MERIDA (not shown), which presents a more uniform wind field (see Figure 17).

Finally, despite the elevation adjustments just described, a substantial negative bias persists for Col della Gallina during the first and last hours considered. This can likely be attributed to changes in the wind directions, which modify the interaction of the flow with the terrain topography.

3.2.3 | The Arbus fire on 31 July 2017

MERIDA HRES does not provide output variables that quantify fire hazard. Nevertheless, we wanted to add an example of using MERIDA HRES to calculate a derived output from a mix of weather variables so that the utility of a physically based reanalysis in quantifying a derived physical process can be explored.

To do that, the Fire Weather Index (FWI) (Van Wagner & Pickett, 1985) is used to quantify fire danger, starting from meteorological fields. In particular, the computation of the FWI requires the temperature and relative humidity fields at 2 m, the wind speed field at 10 m (all calculated at local noon), and the precipitation field accumulated over the previous 24 h. For a detailed explanation of the calculation of the FWI and its

components, the reader is referred to Lawson and Armitage (2008). The FWI has been chosen because it provides an estimate of the potential for wildfire spread from weather variables, and it is one of the most widely used fire indices by forest fire control agencies, including the European Forest Fire Information System (EFFIS) (San-Miguel-Ayanz et al., 2018).

The comparison between the calculated FWI and the effective realization of a wildfire in that area was performed via the EFFIS Burned Area Dataset, which includes the burned area for most wildfires over the past 20 years (Camia et al., 2014) and it is publicly available on the EFFIS website (European Forest Fire Information System, 2024).

The FWI was calculated for the Arbus fire, which took place on the western coast of Sardinia on 31 July 2017 and involved more than 2300 ha of terrain (Figure 19). It took approximately 24 h to extinguish the fire, involving the dispatchment of three Canadair planes and five helicopters. Despite its short lifespan, it has caused the death of many farm animals, severely wounded three people, and caused damage to land and infrastructure for an estimated 20 M€ (VistaNET, 2017).

From a meteorological standpoint, this event is a typical summer wildfire characterized by a long drought before the event, extreme temperatures, and strong, dry katabatic winds. Station observations of the conditions before the fire describe a drought and extremely high temperatures, although not too far from July climatology (Figure 20). Local newspapers mentioned strong winds from the south-eastern direction (Sirocco) (La Nuova Sardegna, 2017; VistaNET, 2017), but the ARPA network does not have enough anemometers in the area to provide experimental feedback.

The FWI was calculated for that day using MERIDA HRES, MERIDA, and ERA5 (Figure 21). As shown, the low resolution of ERA5 does not capture the geographic features of the area, making it unsuitable for analyzing a local event like the Arbus wildfire. Therefore, the rest of
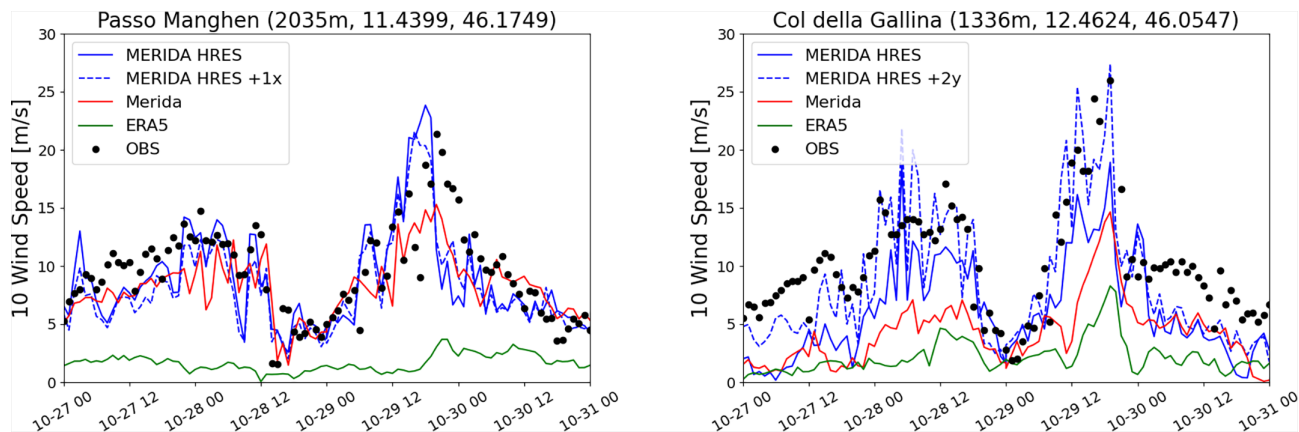
FIGURE 18   Wind speed timeseries during the Vaia storm event for the ARPA stations Passo Manghen and Col della Gallina. Observations (black dots) are compared with model data extracted from the corresponding nearest grid cell (solid lines) and, for MERIDA HRES, from grid cells with closer elevations to those of the stations (dashed lines).

FIGURE 19   Satellite true color images from the SENTINEL-2 constellation before (left panel) and after (center panel) the 2017-07-31 Arbus fire. In the right panel, the burned area from the EFFIS burned area dataset is shown, with the suspected area of ignition indicated by the red triangle.
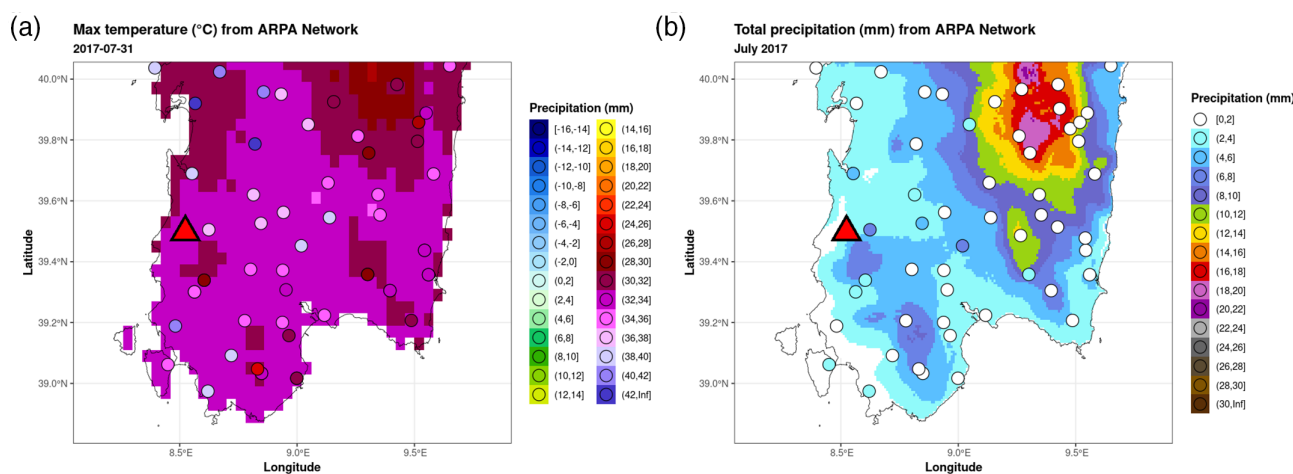

FIGURE 20   Panel A shows the maximum temperatures reached on the day of the event (31 July 2017) as registered by the ARPA network (colored dots). In the background, the average maximum temperature for the month of July is shown, as calculated in Brunetti et al. (2014), using the years 1991–2020 as a reference and the MERIDA HRES 4-km grid. Panel B shows the accumulated rainfall over the month of July 2017 as registered by the ARPA network. In the background, the average accumulated rainfall for July is shown, as calculated in Brunetti et al. (2012) using the years 1991–2020 as a reference. The position of the Arbus wildfire event is marked by a red triangle.
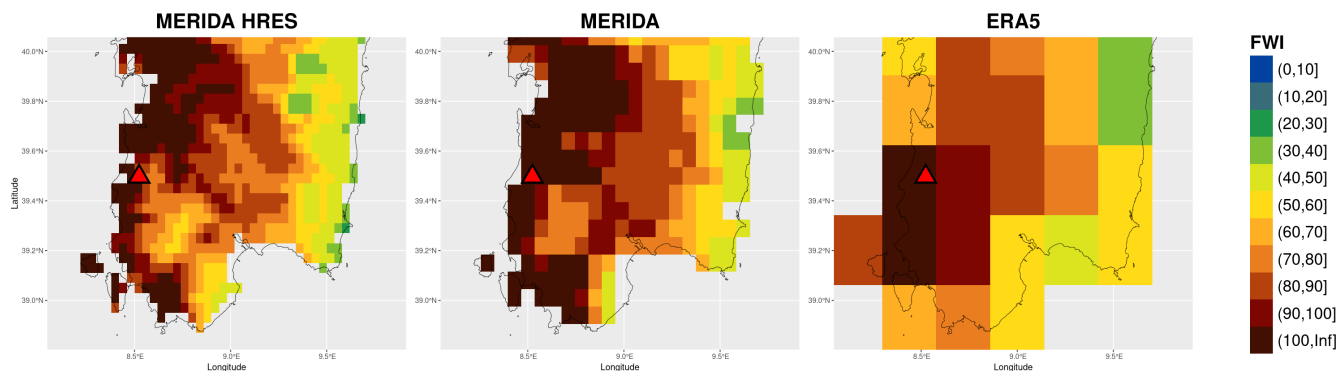
FIGURE 21 FWI index over southern Sardinia for the day (2017–07–31) of the Arbus wildfire event, as calculated using MERIDA HRES, MERIDA, and ERA5. The position of the event is marked by a red triangle.
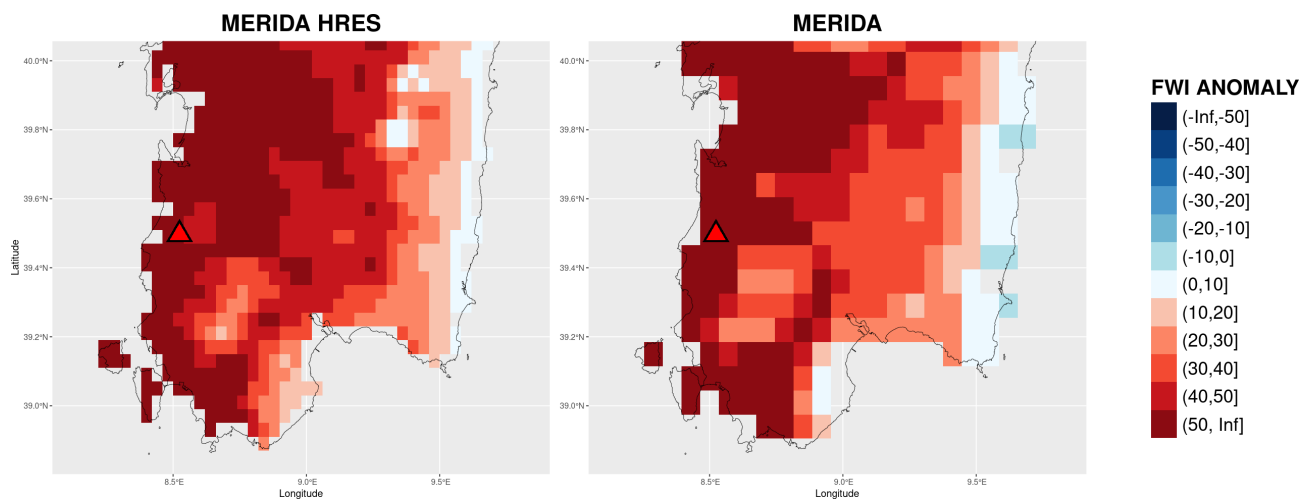

FIGURE 22 FWI index anomaly over southern Sardinia for the day (2017–07–31) of the Arbus wildfire event, as calculated using MERIDA HRES and MERIDA. The anomaly is calculated with respect to the 2005–2020 average FWI in July as a reference. The position of the event is marked by a red triangle.

this discussion will focus on MERIDA and MERIDA HRES. Both products show similar FWI values, with MERIDA covering a larger area with FWI values over 100, while MERIDA HRES assigns similarly high values to a more localized area where the fire actually occurred. These values are extreme, even for a wildfire-prone region, as illustrated by the FWI anomaly in Figure 22, which compares event-day values with the July 2005–2020 average. The atmospheric variables used to calculate the FWI (Figure 23) indicate very high noon temperatures (34–36°C) in both MERIDA and MERIDA HRES, minimal precipitation (with MERIDA HRES producing slightly more), and strong winds concentrated over the fire area in MERIDA HRES. Both reanalyses successfully reproduced high fire risk, but MERIDA HRES offered a more localized and detailed depiction, particularly over the western coast, better capturing orographic influences on the FWI distribution.

In conclusion, while the variable fields may vary between the different reanalyses considered, they all describe an extremely fire-prone situation on the day of the event. This is confirmed by many testimonies as well as the fire warning issued by the regional civil protection.

4 | CONCLUSIONS

This work presents an evaluation and validation of the MERIDA HRES reanalyses product over Italy, comparing it against the MERIDA reanalyses and the ERA5 global reanalyses, which also serves as the driver of both MERIDA HRES and MERIDA.

The analyses are carried out for multiple variables (temperature, precipitation, wind), evaluating different scales, from climatology to individual event cases.
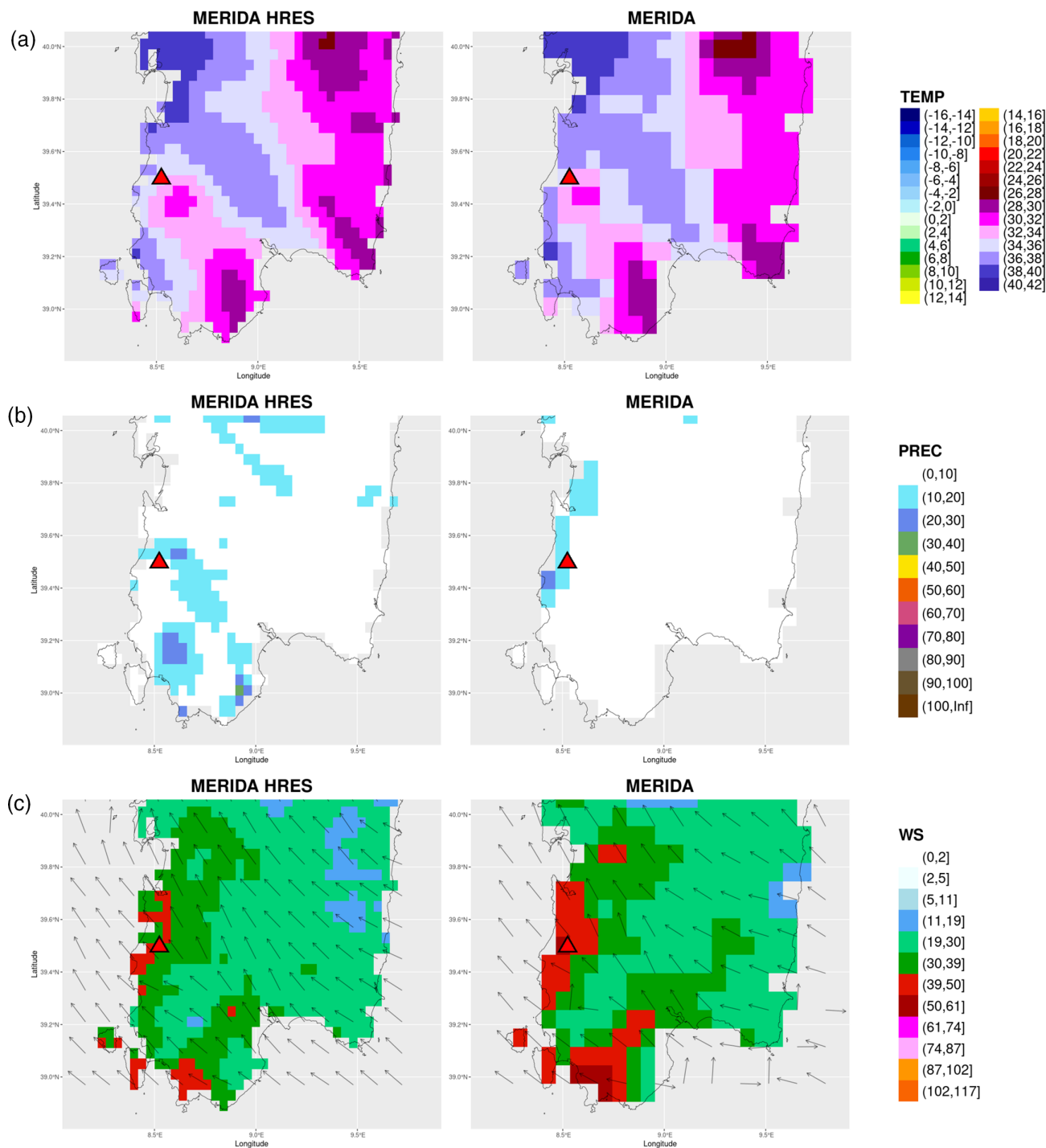
FIGURE 23 Panel A shows the local noon temperature over southern Sardinia for 31 July 2017 of the Arbus wildfire event, as calculated using MERIDA HRES and MERIDA. Panel B shows accumulated rainfall over southern Sardinia for the month (July 2017) of the Arbus wildfire event, as calculated using MERIDA HRES and MERIDA. Panel C shows the wind speed and direction over southern Sardinia for the day (2017-07-31) of the Arbus wildfire event, as calculated using MERIDA HRES and MERIDA.

Multiple techniques are used for the study, comparing both gridded and station observations.

The results highlight a cold bias of more than $-1°C$ associated with MERIDA HRES for all seasons, months, and hours of the day throughout the analyzed period and across the validation techniques used, with a more pronounced underestimation over the orography of the Alps and Apennines. Nevertheless, it reproduces anomalies reasonably well, with correlations comparable to the other two products.

For precipitation, MERIDA HRES achieves the best overall scores, outperforming both MERIDA and ERA5 in summer, likely due its high resolution (4 km) and use of explicit convection, which better captures summer convection. On complex terrain, while MERIDA's skills scores decrease significantly, MERIDA HRES is able to resolve rainfall interactions with the orography, maintaining its performance in such areas. Additionally, MERIDA HRES performs better for higher precipitation thresholds, making it particularly suitable for studying extreme precipitation events.

For wind, both MERIDA HRES and MERIDA show no performance decrease with terrain elevation, unlikeERA5. MERIDA HRES slightly outperforms MERIDA.

Finally, the event-scale analyses support the climatological findings, showing MERIDA HRES improves precipitation performance. In the case of the localized multicell intense precipitation event near Bergamo on July 31, 2016, there is strong agreement between MERIDA HRES and the gridded and rain gauge observations, both in terms of the main peak and precipitation totals. By contrast, the other products reproduced a less intense, more widespread storm with generally lower precipitation amounts.

The analyses of a more synoptically driven event (the Vaia storm) highlights MERIDA HRES's enhanced capability to reproduce the strong variability of the wind field and its interaction with the topography. Wind speed was less underestimated than in MERIDA and ERA5, particularly at the Col del la Galina location.

Lastly, the Arbus wildfire case offered the opportunity to show that it is possible to use MERIDA HRES weather variables to calculate a derived quantity, such as the FWI. Despite the cold bias in t2m, the FWI calculated from MERIDA HRES correctly indicated an extremely fire-prone situation over the Arbus fire area. It also accurately modeled the wind direction that drove the fire and shaped the burned area.

These analyses aim to shed light on the strengths and weaknesses of this new reanalysis product, providing guidance to potential users on its optimal use, depending on the variables and timescales that they wish to analyze.

AUTHOR CONTRIBUTIONS

Francesca Viterbo: Writing – original draft; writing – review and editing; conceptualization; methodology; validation; supervision; formal analysis; investigation; data curation; project administration. **Simone Sperati:** Conceptualization; validation; visualization; writing – original draft; data curation; formal analysis; investigation; methodology. **Bruno Vitali:** Validation; visualization; writing – original draft; formal analysis; investigation. **Filippo D'Amico:** Validation; visualization; formal analysis; writing – original draft; investigation. **Francesco Cavalleri:** Writing – original draft; validation; formal analysis; investigation. **Riccardo Bonanno:** Data curation; conceptualization; methodology; writing – original draft; writing – review and editing; investigation. **Matteo Lacavalla:** Conceptualization; methodology; data curation; supervision; resources; project administration; writing – original draft; writing – review and editing; funding acquisition; investigation.

CONFLICT OF INTEREST STATEMENT

The authors declare no conflicts of interest.

DATA AVAILABILITY STATEMENT

ERA5 is downloadable at https://cds.climate.copernicus.eu/. MERIDA and MERIDA HRES datasets are available at http://merida.rse-web.it/. ARCIS dataset is available at https://www.arcis.it/wp/. The UniMi/ISAC-CNR gridded observational datasets are available upon request. ARPA station observations are retrieved trough the Italian Civil Protection Agency portal, made possible through a specific collaboration agreement with RSE S.p.A., in the framework of the Research Fund for the Italian Electrical System project for Resilience and Security of Energy System.

ORCID

Francesca Viterbo https://orcid.org/0000-0002-3600-6661

REFERENCES

Abbate, A., Mancusi, L., Apadula, F., Frigerio, A., Papini, M. & Longoni, L. (2024) CRHyME (climatic rainfall hydrogeological modelling experiment): a new model for geo-hydrological hazard assessment at the basin scale. *NHESS*, 24(2), 501–537.

Amicarelli, E., Marcacci, P., de Masi, M., Lacavalla, M. & Valtorta, G. (2019) Impact of snow storms on distribution grids: e-distribuzione and RSE experimental stations. In *2019 AEIT international annual conference (AEIT)*, IEEE. pp. 1–6.

Anderson, J.R., Hardy, E.E., Roach, J.T. & Witmer, R.E. (1976) *A land use and land cover classification system for use with remote sensor data*. s.l.:US Government Printing Office.

ARERA. (2017) *Deliberation 645/25 September 2017/R/eel*. Available at: https://www.arera.it/atti-e-provvedimenti Accessed on 21 March 2024.

Auer, I., Böhm, R., Jurkovic, A., Lipa, W., Orlik, A., Potzmann, R. et al. (2007) HISTALP—historical instrumental climatological surface time series of the greater alpine region. *International Journal of Climatology: A Journal of the Royal Meteorological Society*, 27(1), 17–46.

Bloomfield, H.C., Gonzalez, P.L.M., Lundquist, J.K., Stoop, L.P., Browell, J., Dargaville, R. et al. (2021) The importance of weather and climate to energy systems: a workshop on next generation challenges in energy–climate modeling. *Bulletin of the American Meteorological Society*, 102(1), E159–E167.

Bonanno, R. & Lacavalla, M. (2020) A feasibility analysis aimed at defining an alert system for distribution MV underground cables. In *2020 AEIT International Annual Conference (AEIT)*, IEEE, pp. 1–6.

Bonanno, R., Lacavalla, M. & Sperati, S. (2019) A new high-resolution meteorological reanalysis Italian dataset: MERIDA. *Quarterly Journal of the Royal Meteorological Society*, 145(721), 1756–1779.

Bonanno, R., Viterbo, F. & Maurizio, R.G. (2023) Climate change impacts on wind power generation for the Italian peninsula. *Regional Environmental Change*, 23(1), 15.

Brunetti, M., Lentini, G., Maugeri, M., Nanni, T., Simolo, C. & Spinoni, J. (2012) Projecting North Eastern Italy temperature and precipitation secular records onto a high-resolution grid. *Physics and Chemistry of the Earth, Parts A/B/C*, 40, 9–22.

Brunetti, M., Maugeri, M., Nanni, T., Simolo, C. & Spinoni, J. (2014) High-resolution temperature climatology for Italy: interpolation method intercomparison. *International Journal of Climatology*, 34(4), 1278–1296.

Camargo, L.R., Gruber, K. & Nitsch, F. (2019) Assessing variables of regional reanalysis data sets relevant for modelling small-scale renewable energy systems. *Renewable Energy*, 133, 1468–1478.

Camia, A., Durrant, T. & San-Miguel-Ayanz, J. (2014) *The European fire database: technical specifications and data submission*. EUR 26546 EN. Luxemburg: Publications Office of the European Union.

Capozzi, V., Annella, C. & Budillon, G. (2023) Classification of daily heavy precipitation patterns and associated synoptic types in the Campania Region (Southern Italy). *Atmospheric Research*, 289, 106781.

Cavalleri, F., Viterbo, F., Brunetti, M., Bonanno, R., Manara, V., Lussana, C., Lacavalla, M., and Maugeri, M., 2024. *Inter-comparison and validation of high-resolution surface air temperature reanalysis fields over Italy. International Journal of Climatology*, 44(8), 2681–2700.

Cerenzia, I.M.L., Giordani, A., Paccagnella, T. & Montani, A. (2022) Toward a convection-permitting regional reanalysis over the Italian domain. *Meteorological Applications*, 29(5), e2092.

Cleveland, W.S., Grosse, E. & Shyu, W.M. (1992) Local regression models. In J.M. Chambers & T.J. Hastie (Eds.) *Statistical models in S.,* Pacific Grove, CA: Wadsworth & Brooks/Cole, pp. 309–376.

Craig, M.T., Wohland, J., Stoop, L.P., Kies, A., Pickering, B., Bloomfield, H.C. et al. (2022) Overcoming the disconnect between energy system and climate modeling. *Joule*, 6(7), 1405–1417.

Crespi, A., Brunetti, M., Lentini, G. & Maugeri, M. (2018) 1961–1990 high-resolution monthly precipitation climatologies for Italy. *International Journal of Climatology*, 38(2), 878–895.

Dubus, L., Saint-Drenan, Y.M., Troccoli, A., De Felice, M., Moreau, Y., Ho-Tran, L. et al. (2023) C3S energy: a climate service for the provision of power supply and demand indicators for Europe based on the ERA5 reanalysis and ENTSO-E data. *Meteorological Applications*, 30(5), e2145.

Dueben, P.D. & Bauer, P. (2018) Challenges and design choices for global weather and climate models based on machine learning. *Geoscientific Model Development*, 11(10), 3999–4009.

Ebert, E.E. (2008) Fuzzy verification of high-resolution gridded forecasts: a review and proposed framework. *Meteorological Applications: A Journal of Forecasting, Practical Applications, Training Techniques and Modelling*, 15(1), 51–64.

European Forest Fire Information System. *Data and services.* Available at: https://forest-fire.emergency.copernicus.eu/applications/data-and-services [Accessed on 3 June 2024].

Faggian, P., Decimi, G., Ciapessoni, E., Marzullo, F. & Scavo, F. (2021) Future projections and return levels of wet-snow load on overhead lines and heavy snowfalls. In *2021 AEIT International Annual Conference (AEIT)*, IEEE. pp. 1–6.

Faggian, P. & Trevisiol, A. (2024) Climate extreme scenarios affecting the Italian energy system with a multi-hazard approach. *Bulletin of Atmospheric Science and Technology*, 5(1), 4.

Faggian, P., Trevisiol, A. & Decimi, G. (2024) Future projections of wet snow frequency and wet snow load on overhead high voltage conductors over Italy. *Cold Regions Science and Technology*, 217, 103980.

Giannetti, F., Pecchi, M., Travaglini, D., Francini, S., D'Amico, G., Vangi, E. et al. (2021) Estimating VAIA windstorm damaged forest area in Italy using time series Sentinel-2 imagery and continuous change detection algorithms. *Forests*, 12(6), 680.

Giovannini, L., Davolio, S., Zaramella, M., Zardi, D. & Borga, M. (2021) Multi-model convection-resolving simulations of the October 2018 Vaia storm over Northeastern Italy. *Atmospheric Research*, 253, 105455.

González-Hidalgo, J.C., Brunetti, M. & De Luis, M. (2011) A new tool for monthly precipitation analysis in Spain: MOPREDAS database (monthly precipitation trends December 1945–November 2005). *International Journal of Climatology*, 31(5), 715–731.

Haiden, T., Rodwell, M.J., Richardson, D.S., Okagaki, A., Robinson, T. & Hewson, T. (2012) Intercomparison of global model precipitation forecast skill in 2010/11 using the SEEPS score. *Monthly Weather Review*, 140(8), 2720–2733.

Hanssen, A.W. & Kuipers, W.J.A. (1965) On the relationship between the frequency of rain and various meteorological parameters: (with references to the problem of objective forecasting). Mededeelingen en Verhandelingen, 81, 2–15.

Hersbach, H., Bell, B., Berrisford, P., Hirahara, S., Horányi, A., Muñoz-Sabater, J. et al. (2020) The ERA5 global reanalysis. Quarterly Journal of the Royal Meteorological Society, 146(730), 1999–2049.

Hong, S.Y., Noh, Y. & Dudhia, J. (2006) A new vertical diffusion package with an explicit treatment of entrainment processes. Monthly Weather Review, 134(9), 2318–2341.

Honnert, R., Efstathiou, G.A., Beare, R.J., Ito, J., Lock, A., Neggers, R. et al. (2020) The atmospheric boundary layer and the "gray zone" of turbulence: a critical review. Journal of Geophysical Research: Atmospheres, 125(13), e2019JD030317.

Iacono, M.J., Delamere, J.S., Mlawer, E.J., Shephard, M.W., Clough, S.A. & Collins, W.D. (2008) Radiative forcing by long-lived greenhouse gases: calculations with the AER radiative transfer models. Journal of Geophysical Research: Atmospheres, 113(D13103).

Isotta, F.A., Frei, C., Weilguni, V., Perčec Tadić, M., Lassegues, P., Rudolf, B. et al. (2014) The climate of daily precipitation in the Alps: development and analysis of a high-resolution grid dataset from pan-alpine rain-gauge data. International Journal of Climatology, 34(5), 1657–1675.

Italian Civil Protection Department and CIMA Research Foundation. (2014) The Dewetra platform: a multi-perspective architecture for risk management during emergencies. In: Information Systems for Crisis Response and Management in Mediterranean countries: first international conference, ISCRAM-med 2014, Toulouse, France, October 15–17, 2014. Proceedings 1. New York: Springer International Publishing, pp. 165–177.

Jermey, P.M. & Renshaw, R.J. (2016) Precipitation representation over a two-year period in regional reanalysis. Quarterly Journal of the Royal Meteorological Society, 142(696), 1300–1310.

Jiménez, P.A. & Dudhia, J. (2012) Improving the representation of resolved and unresolved topographic effects on surface wind in the WRF model. Journal of Applied Meteorology and Climatology, 51(2), 300–316.

Jiménez, P.A., Dudhia, J., González-Rouco, J.F., Navarro, J., Montávez, J.P. & García-Bustamante, E. (2012) A revised scheme for the WRF surface layer formulation. Monthly Weather Review, 140(3), 898–918.

Ju, C., Li, H., Li, M., Liu, Z., Ma, Y., Mamtimin, A. et al. (2022) Comparison of the forecast performance of WRF using Noah and Noah-MP land surface schemes in Central Asia arid region. Atmosphere, 13(6), 927.

Kalnay, E. (1996) The NCEP/NCAR 40-yr reanalysis project. Bulletin of the American Meteorological Society, 77, 431–477.

Kies, A., Schyska, B.U., Bilousova, M., El Sayed, O., Jurasz, J. & Stoecker, H. (2021) Critical review of renewable generation datasets and their implications for European power system models. Renewable and Sustainable Energy Reviews, 152, 111614.

Lacavalla, M., Marcacci, P., Bonanno, R. & Sperati, S. (2022) Updates on research activities of wet snowfalls in Italy: snow load map reanalysis, forecasting and monitoring. In Proceedings – International workshop on atmospheric icing of structures, IWAIS, Montreal, Canada, pp. 1–8.

Lacavalla, M., Sperati, S., Bonanno, R. & Marcacci, P. (2019) A revision of wet snow load map for the Italian power lines with a new high resolution reanalysis dataset. In Proceedings of the International Workshop on Atmopheric Icing of Structures, IWAIS, Reykjavik, Iceland. pp. 23–28.

Lanciani, A., Mariani, S., Casaioli, M., Accadia, C. & Tartaglione, N. (2008) A multiscale approach for precipitation verification applied to the FORALPS case studies. Advances in Geosciences, 16, 3–9.

Lawson, B.D. and Armitage, O.B., 2008. Weather guide for the Canadian forest fire danger rating system. Edmonton, AB: Natural Resources Canada, Canadian Forest Service.

Luo, H., Ge, F., Yang, K., Zhu, S., Peng, T., Cai, W. et al. (2019) Assessment of ECMWF reanalysis data in complex terrain: can the CERA-20C and ERA-interim data sets replicate the variation in surface air temperatures over Sichuan, China? International Journal of Climatology, 39(15), 5619–5634.

Miller, D.A. & White, R.A. (1998) A conterminous United States multilayer soil characteristics dataset for regional climate and hydrology modeling. Earth Interactions, 2(2), 1–26.

Mitchell, K. (2005) The community Noah land-surface model (LSM). User's Guide Public Release Version, 2(1). Available at: https://ral.ucar.edu/document-or-file/noah-lsm-users-guide Accessed on 27 March 2024.

Mitchell, T.D. & Jones, P.D. (2005) An improved method of constructing a database of monthly climate observations and associated high-resolution grids. International Journal of Climatology: A Journal of the Royal Meteorological Society, 25(6), 693–712.

Niu, G.Y., Yang, Z.L., Mitchell, K.E., Chen, F., Ek, M.B., Barlage, M. et al. (2011) The community Noah land surface model with multiparameterization options (Noah-MP): 1. Model description and evaluation with local-scale measurements. Journal of Geophysical Research: Atmospheres, 116(D12109).

Raffa, M., Reder, A., Marras, G.F., Mancini, M., Scipione, G., Santini, M. et al. (2021) VHR-REA_IT dataset: very high resolution dynamical downscaling of ERA5 reanalysis over Italy by COSMO-CLM. Data, 6(8), 88.

Raimonet, M., Oudin, L., Thieu, V., Silvestre, M., Vautard, R., Rabouille, C. et al. (2017) Evaluation of gridded meteorological datasets for hydrological modeling. Journal of Hydrometeorology, 18(11), 3027–3041.

Rodwell, M.J., Richardson, D.S., Hewson, T.D. & Haiden, T. (2010) A new equitable score suitable for verifying precipitation in numerical weather prediction. Quarterly Journal of the Royal Meteorological Society, 136(650), 1344–1363.

Roebber, P.J. (2009) Visualizing multiple measures of forecast quality. Weather and Forecasting, 24(2), 601–608.

Ruiz-Arias, J.A., Dudhia, J., Lara-Fanego, V. & Pozo-Vázquez, D. (2013) A geostatistical approach for producing daily Level-3 MODIS aerosol optical depth analyses. Atmospheric Environment, 79, 395–405.

San-Miguel-Ayanz, J., Costa, H., De, R., Libertà, G., Artes, V.T., Durrant, H.T. et al. (2018) Basic criteria to assess wildfire risk at the pan-European level.

La Nuova Sardegna. (2017) Un indagato per l'incendio di Gonnosfanadiga e Arbus. Available at: https://www.lanuovasardegna.it/cagliari/cronaca/2017/08/14/news/un-indagato-per-l-incendio-di-gonnosfanadiga-e-arbus-1.15733135 [Accessed on 10 June 2024]

Skamarock, W.C., Klemp, J.B., Dudhia, J., Gill, D.O., Barker, D.M., Duda, M.G. et al. (2008) A description of the advanced research WRF version 3. *NCAR Technical Note*, 475, 113.

Sperati, S., Alessandrini, S., D'Amico, F., Cheng, W., Rozoff, C.M., Bonanno, R. et al. (2024) A new wind atlas to support the expansion of the Italian wind power fleet. *Wind Energy*, 27, 298–316.

Stefanini, C., Becherini, F., Della Valle, A., Rech, F., Zecchini, F. & Camuffo, D. (2023) Homogeneity assessment and correction methodology for the 1980–2022 daily temperature series in Padua, Italy. *Climate*, 11(12), 244.

Thompson, G., Field, P.R., Rasmussen, R.M. & Hall, W.D. (2008) Explicit forecasts of winter precipitation using an improved bulk microphysics scheme. Part II: implementation of a new snow parameterization. *Monthly Weather Review*, 136(12), 5095–5115.

Tian, Y., Huffman, G.J., Adler, R.F., Tang, L., Sapiano, M., Maggioni, V. et al. (2013) Modeling errors in daily precipitation measurements: additive or multiplicative? *Geophysical Research Letters*, 40(10), 2060–2065.

Tipton, E. & Seitter, K.L. (2022) *Actionable scientific assessments for the energy sector. An AMS policy program study*. Washington, DC: The American Meteorological Society. Available from: https://doi.org/10.1175/energy-sector-assessment-2022

Troccoli, A., Dubus, L. & Haupt, S.E. (Eds.). (2014) *Weather matters for energy (Vol. 528)*. New York: Springer.

Van Wagner, C.E. & Pickett, T.L. (1985) Equations and FORTRAN program for the Canadian forest fire weather index system, 33.

Verrelle, A., Glinton, M., Bazile, E., Le Moigne, P., Randriamampianina, R., Ridal, M. et al. (2022) *CERRA-land sub-daily regional reanalysis data for Europe from 1984 to present*. Reading: Copernicus Climate Change Service (C3S) Climate Data Store (CDS).

Victoria, M. & Andresen, G.B. (2019) Using validated reanalysis data to investigate the impact of the PV system configurations at high penetration levels in European countries. *Progress in Photovoltaics: Research and Applications*, 27(7), 576–592.

VistaNET. (2017) Arbus e Gonnosfanadiga, le foto degli animali morti nel terribile incendio di ieri. *Allevatori in ginocchio*. Available at: https://www.vistanet.it/cagliari/2017/08/01/arbus-e-gonnosfanadiga-le-foto-degli-animali-morti-nel-terribile-incendio-di-ieri-allevatori-in-ginocchio/ Accessed on 10 June 2024.

von Storch, H., Langenberg, H. & Feser, F. (2000) A spectral nudging technique for dynamical downscaling purposes. *Monthly Weather Review*, 128(10), 3664–3673.

Wayne, W.D. (1990) Kolmogorov–Smirnov one-sample test. In: *Applied nonparametric statistics*, 2nd edition. Boston: PWS-Kent, pp. 319–330.

Weisman, M.L., Skamarock, W.C. & Klemp, J.B. (1997) The resolution dependence of explicitly modeled convective systems. *Monthly Weather Review*, 125(4), 527–548.

Weyn, J.A., Durran, D.R. & Caruana, R. (2019) Can machines learn to predict weather? Using deep learning to predict gridded 500-hPa geopotential height from historical weather data. *Journal of Advances in Modeling Earth Systems*, 11(8), 2680–2693.

Wyngaard, J.C. (2004) Toward numerical modeling in the "Terra Incognita". *Journal of the Atmospheric Sciences*, 61(14), 1816–1826.

Yang, Z.L., Niu, G.Y., Mitchell, K.E., Chen, F., Ek, M.B., Barlage, M. et al. (2011) The community Noah land surface model with multiparameterization options (Noah-MP): 2. Evaluation over global river basins. *Journal of Geophysical Research: Atmospheres*, 116(D12110).

SUPPORTING INFORMATION

Additional supporting information can be found online in the Supporting Information section at the end of this article.